IEEE Access
Multidisciplinary | Rapid Review | Open Access Journal

Received December 23, 2020, accepted January 10, 2021, date of publication January 25, 2021, date of current version February 2, 2021.

Digital Object Identifier 10.1109/ACCESS.2021.3054532

Multi-Objective Optimization Strategy of Integrated Electric-Heat System Based on Energy Storage Situation Division

XINRUI LIU, (Member, IEEE), FUJIA ZHANG, QIUYE SUN, (Senior Member, IEEE), AND WEIYANG ZHONG

College of Information Science and Engineering, Northeastern University, Shenyang 110819, China

Corresponding author: Xinrui Liu (liuxinrui@ise.neu.edu.cn)

This work was supported in part by the National Key Research and Development Program of China under Grant 2018YFA0702200 and Grant 2018YFB1700500, and in part by the Fundamental Research Funds for the Central Universities under Grant N2004013.

ABSTRACT There are the transmission loss of the electric power network, the delay and loss of the heating network, the insufficient utilization of flexible resources such as energy storage in the integrated electric-heat system, which may lead to the imbalance of supply and demand and energy waste. In this paper, the coordinated dispatch of integrated electric-heat system (IEHS) considering the transmission characteristics of the electric power network and heating network, which is formulated as a convex quadratic program. The strong linkage of electric power and heat supplies can be decoupled to reduce wind power curtailment by exploiting the energy storage and regulation capabilities of the district heating network (DHN), storage batteries, electric boilers (EBs) and heat storage tanks (HSs). The energy storage system works according to the situation division strategy designed in this paper. This paper introduces the wind curtailment boundary power and optimizes dispatch based on the wind curtailment boundary power and unit output, which can make full use of the energy storage capacity and reduce the wind abandonment power. Since the electric power system (EPS) and the distribution heating system (DHS) are controlled separately by different operation organizations, IEHS is solved using double-λ iterative algorithm. The double-λ iterative algorithm, with guaranteed convergence for convex programs, can achieve a fully distributed solution for the IEHS and requires only a small amount boundary information exchange between the EPS and the DHS. At last, one integrated electric-heat system was studied to demonstrate the effectiveness of the proposed method which achieves the effective solution in a moderate number of iterations. This system includes two 10-nodes heating system and one 14-nodes electric power system.

INDEX TERMS Integrated electric-heat system, energy storage situation, network transmission characteristics, wind power accommodation, double-λ iterative algorithm.

I. INTRODUCTION

In recent years, China's energy structure has been continuously adjusted with energy and environmental problems. Distributed power sources and energy storage equipment have continued to emerge. Wind power resources are rapidly expanding in scale which as a clean, pollution-free, high-quality renewable new energy. A combined heat and power (CHP) unit has the ability to produce electricity and heat simultaneously. The fuel efficiency of a CHP unit can reach 90%, while that of conventional thermal units is only 60% [1]. Due to its high efficiency, CHP units are more environmentally friendly than conventional thermal units [2], [3]. However, because the output of CHP units is routinely determined by the heat loads, so wind power generation is restricted, especially in winter, when the electricity demand is low but the heat load is high [4].

One direct solution to increase the operational flexibility of the CHP and reduce wind curtailment is to install storage batteries [5], EBs [6], [7] and HSs [8]. The energy storage equipment has the functions of time-shifting and storage of energy which has been widely applied and promoted [9].

The associate editor coordinating the review of this manuscript and approving it for publication was Shuaihu Li.

Another solution is to consider the pipeline energy storage and transmission characteristics of the DHN which does not require additional investment [10]. Due to the transmission delay and loss of the district heating network, the transmission loss of the electric power network, which will seriously affect the accuracy of system scheduling. By considering the transmission characteristics of the district heating network and the power network, coordination of the electric power system and heating system can effectively increase the regulation flexibility and enhance the utilization of wind power. The energy storage system adopts the situation division strategy designed in this paper to work, introduces the wind curtailment boundary power and optimizes dispatch based on the wind curtailment boundary power and unit output, which can make full use of the energy storage capacity and reduce the wind abandonment power.

There may be a number of small DHSs in different districts and only one EPS in a large area, such as a city. Actually, the DHSs and the EPS have different control center and they are controlled separately by different operating organizations without a coordinator. As shown in Figure 1, an integrated electric-heat system is composed of the EPS and the DHSs. The EPS consists of traditional thermal units, wind turbines, storage batteries, electric loads and transmission lines which is controlled by the electricity control center (ECC). A DHS is managed by the district heating control center (HCC) which is composed of heat-exchanger stations, insulated hot-water pipelines and heat loads, as well as heat sources, including CHP units, EBs, and heat storage tanks. Some information must be exchanged between the ECC and HCCs to achieve coordination in the dispatch of an integrated electric-heat system. However, it does not require the information exchange between the district heating control centers.

In recent years, extensive work has been conducted on the coordinated optimization of integrated electric-heat system, the emergence of intelligent algorithms has solved this problem. For example, particle swarm algorithm [11]–[13], genetic algorithm [14], ant colony search algorithm [15], harmonic search algorithm [16] and group search optimizer [17], [18] all can be used to solve the coordination and optimization of integrated electric-heat system. However, the common defects of intelligent algorithms are that the computation time is long and it is difficult to use them in real-time applications. Another type of solution method is based on mathematical programming techniques. For example, the application of the branch and bound algorithm for combined heating, cooling and power dispatch is presented in [19]. Some novel algorithms including the feasible region method [20] and the mixed-integer linear programming algorithm [21] have also been employed to solve this problem. A two-layer algorithm is proposed in [22] to solve the combined heat and power economic dispatch problem, but the computation efficiency of the algorithm is not demonstrated in real systems. The paper [23] introduces a decomposition-coordination algorithm to solve the optimal operation of the integrated electrical and heating systems; however, no proof of convergence is presented. Moreover, the pipeline energy storage of the DHN is not considered in [22], [23].

This paper proposes an efficient double-λ iterative algorithm to solve the electric-heat network coordination problem which considering the transmission characteristics of the electric-heating network. The double-λ iterative algorithm has been successfully implemented to solve a number of optimization problems in power systems, such as the optimal power flow problem [25], [26]. In addition, the double-λ iterative algorithm can be used to solve the dynamic economic dispatch problem [27] and multi-area energy and reserve dispatch under wind uncertainty and equipment failures [28]. The double-λ iterative algorithm requires only minor boundary information to be exchanged without any central coordination. Hence, the double-λ iterative algorithm is simple, efficient and practical [28]. Most importantly, the double-λ iterative algorithm can guarantee the privacy of data during decision making and achieve a fully distributed solution for the coordinated optimization problem.

The main contributions of this paper are as follows:

1) A coordination model for integrated electric-heat system is proposed to adapt to conditions where the EPS and DHSs are controlled separately by different operating organizations.
2) Wind curtailment boundary power is defined, and the situation division method for the energy storage system is proposed, which can optimize dispatching according to each energy storage state to maximize the utilization of energy storage.
3) Aiming at several typical components of urban electric and heating systems, such as electric boilers, heat storage tanks and storage batteries, a coordinated optimization method for the integrated electric-heat system considering the characteristics of network transmission is proposed. The proposed model is convex with linear constraints, the solution of which is computationally tractable.
4) A solution is proposed based on the double-λ iterative algorithm, which is simple and efficient, does not require central coordinator and involves only a small amount boundary information exchange between the EPS and the DHSs.

II. STRUCTURE AND COORDINATION MODE OF INTEGRATED ELECTRIC-HEAT SYSTEM

A typical integrated electric-heat systems structure is shown in Figure 1, which includes a power generation part composed of thermal units, wind turbines, CHP units, as well as power grids, heating networks, EBs, HSs, storage batteries, electrical loads and heat loads.

The optimization model of the integrated electric-heat system is established, which can reduce the power deviation of the supply and demand side caused by the delay and loss of network. Moreover, flexibility resources are effectively used

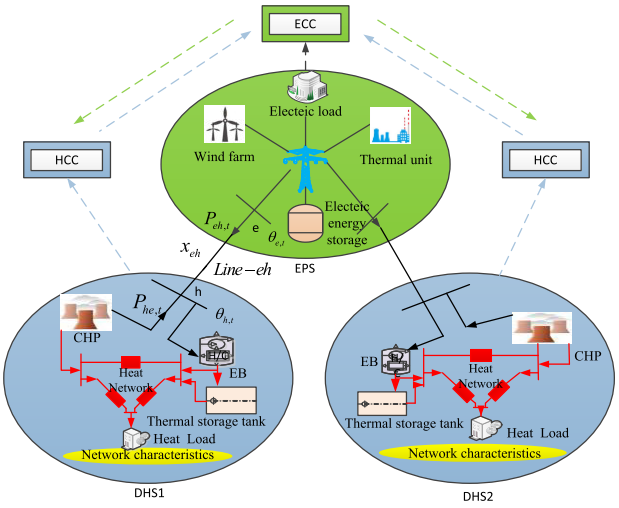

FIGURE 1. Structure diagram of the integrated electric-heat system with energy storage.

in the system optimization process and the utilization of wind power is improved while system operating costs is reduced.

The integrated electric-heat system needs to exchange some information during the coordination period, only the ECC and the HCC need to exchange some information in each coordination period to determine the transmission power on the feeder. The coordination model of the integrated electric-heat system is described in the following sections.

The CHP units are coupled with the EBs, the power flow from DHS to EPS through the feeder can be expressed as equation (1). Generally, in high-voltage lines, AC power flow can be approximately simplified to DC power flow. The power flow constraint of the feeder in this paper is simplified to equation (2), which does not affect the accuracy of the calculation.

$$P_{he,t} = P_{CHP,i,t} - P_{EB,i,t} \tag{1}$$

$$P_{he,t} = \frac{1}{x_{he}}(\theta_{h,t} - \theta_{e,t}) \tag{2}$$

where $P_{he,t}$ is the power flow from h to e on the feeder he in period t. The total electric output of the CHP units of heating system i is $P_{CHP,i,t}$, $P_{EB,i,t}$ is the output power of the wind turbine to the electric boiler of heating system i. $\theta_{e,t}$ and $\theta_{h,t}$ are the voltage phase angles of the bus bar e and bus bar h on the DHS side in period t. The direct current resistance of the feeder is x_{eh}.

Note that if only the CHP units are connected to the border bus in a DHS, the electricity consumptions of EBs are set to zero in Eq. (1). In addition, for the EB plants without CHP units, the power outputs of CHP units are set to zero.

III. ANALYSIS OF TRANSMISSION CHARACTERISTICS OF ELECTRIC-HEAT NETWORK

In the integrated electric-heat system, the balance of active power must be maintained among wind turbines, thermal units, CHP units, EBs, storage batteries and electric loads to keep the grid frequency within the qualified range. The energy loss during the transmission of electric energy constitutes the characteristics of the electric power grid. The heat loss and delay effect of the heat transfer medium in the heat transfer process constitute the characteristics of the heat network.

A. POWER GRID TRANSMISSION CHARACTERISTICS

Equation (3) shows the balance of electrical power of the system.

$$\begin{cases} \Delta P = P_{G,t} + \sum_{i=1}^{M} P_{CHP,i,t} + P_{EES,DIS,t} + P_{W,EL,t} \\ \qquad - P_{EES,CHA,t} - \sum_{i=1}^{M} P_{EB,i,t} - P_{EL,t} - P_{E,t} = 0, \\ \qquad t = 1 \ldots\ldots T \\ P_{G,t} = \sum_{j=1}^{N} P_{G,j,t} \\ P_{EL,t} = \sum_{l=1}^{L} P_{EL,l,t} \end{cases} \tag{3}$$

where ΔP is the system electric power deviation, N is the number of thermal power units, $P_{G,j,t}$ is the electric output of the j-th thermal power unit, M is the number of heating systems, $P_{EES,DIS,t}$ is the storage batteries output power, $P_{W,EL,t}$ is the power supplied by the wind power plant to the electric load end, $P_{EES,CHA,t}$ is the input power of the storage batteries, L is the total number of electric load, $P_{EL,l,t}$ is the demand of the l-th electric load, T is the total scheduling period. $P_{E,t}$ is electric transmission loss of the system, as shown in equation (4) [24], [25].

$$P_{E,t} = \sum_{r=1}^{R}\sum_{m=1}^{R} O_{r,t}B_{rm}O_{m,t} + 2\sum_{r=1}^{R}\sum_{i=1}^{M} O_{r,t}B_{ri}P_{CHP,i,t} + \sum_{i=1}^{M}\sum_{n=1}^{M} P_{CHP,i,t}B_{in}P_{CHP,n,t}, \quad t = 1 \ldots\ldots T \tag{4}$$

where $O_{r,t}$ is the electric output of the rth thermal power unit. B_{rm}, B_{ri} and B_{in} are the corresponding elements of the loss coefficient matrix B. The coefficient of the B matrix satisfies $B_{ri} = B_{ir}$, which can be specifically calculated from the line parameters and the daily operating status of the power system. The system has two types of units, one is pure generator unit, the other is CHP unit. The pure generator units include wind turbines and thermal units, the total number is R.

The output of the wind turbine of the system is shown in equation (5) and the input power of storage batteries satisfies equation (6).

$$P_{W,t} = \sum_{i=1}^{M} P_{EB,i,t} + P_{W,EL,t} + P_{W,EES,t} \tag{5}$$

$$P_{W,EES,t} = P_{EES,CHA,t} \tag{6}$$

where $P_{W,t}$ is the output of the wind turbine of the integrated electric-heat system, $P_{W,EES,t}$ is the output power of the wind turbine to the storage batteries.

B. HEATING NETWORK TRANSMISSION CHARACTERISTICS

Part A discusses the transmission characteristics of the electric network. Here, the transmission loss and delay of the thermal network will be discussed, which has a greater impact on the optimal dispatch of integrated electric-heat system [26]. Equation (7) shows the balance of thermal power of the system.

$$\Delta H_i = H_{CHP,i,t} + H_{EB,HL,i,t} + H_{HS,OUT,i,t} - H_{EV,i,t} - H_{E,i,t} = 0, \quad i = 1 \cdots M, \ t = 1 \ldots T \tag{7}$$

where ΔH_i is the sum of the thermal power deviation of the i-th heating system, MWth, the total thermal output of the CHP units of i-th heating system is $H_{CHP,i,t}$, the thermal power output of the electric boiler direct to heating network of i-th heating system is $H_{EB,HL,i,t}$, the thermal power output released by the heat storage tank to the heating network of the i-th heating system is $H_{HS,OUT,i,t}$, $H_{EV,i,t}$ is the heat load of the i-th heating system, $H_{E,i,t}$ is heat loss of the i-th heating system.

According to the principle of steady-state heat transfer, the thermal loss of the heat medium flowing through a pipe dl_g of a sufficiently small length is shown as equation (8) [26], [27].

$$\Delta H_E = 2\pi \frac{T_g - T_0}{\sum \varepsilon} dl_g \tag{8}$$

where ΔH_E is the heat loss of the heat medium flowing through a unit length of pipe, kW. $l_g$is the length of the heat medium flowing through the pipe g, km. T_g is the temperature of the heat medium in the pipe g,°C. T_0 is the ambient temperature around the pipe, °C. $\sum \varepsilon$ is the total thermal resistance per kilometer of the pipe between the thermal medium and the surrounding medium, km ·° C/kW.

The change of heat energy that contained in the heat medium is related to its temperature drop and flow rate, which is shown as equation (9).

$$\Delta H_E = -3600kmdT \tag{9}$$

where m is the flow rate of the heat medium, m^3/h, k is the constant of proportionality, $k = c\rho$ and c is the specific heat capacity of the heat medium, kJ/(kg ·° C), ρ is the density of the heat medium, kg/m^3.

$H_{E,t}$ is the heat transmission loss of the system, which is shown as equation (10) according to the basic principle of steady-state heat transfer.

$$H_{E,t} = \sum_{g=1}^{n} \Delta H_E \tag{10}$$

where n is the total number of sections of the pipeline that the heat medium flows through.

Combine equation (7) and (8), we take integrals on both sides at the same time, which is shown as equation (11).

$$\int_0^{nl_g} \frac{-2\pi}{km \sum \varepsilon} dl_g = \int_{T_i}^{T_j} \frac{1}{T_g - T_0} dt \tag{11}$$

To simplify the calculation, it is assumed that the external environment temperature is constant, so T_0 and $\sum \varepsilon$ in (11) can be considered as constants and the Sukhov temperature drop formula can be obtained by solving the above equation.

$$T_j = T_i e^{\frac{-2\pi}{km\sum \varepsilon} l} + (1 - e^{\frac{-2\pi}{km\sum \varepsilon} l}) T_0 \tag{12}$$

After sorting out equation (12) and applying it to the heating network, the temperature loss equation of pipeline transmission is shown as equation (13).

$$T_j = (T_i - T_0)\, e^{-\frac{\lambda l_{ij}}{cm_{ij}^h}} + T_0 \tag{13}$$

where T_i and T_j represent the temperature of hot water flowing through nodes i and j respectively, and the flow direction is from node i to node j, l_{ij} represents the length of pipe $i-j$, m_{ij}^h is the water flow of pipe $i-j$, λ is the temperature loss coefficient of the unit length of the pipe which is determined by the nature of the pipe, kW/km°C.

The energy exchange at the heat load node can be expressed as equation (14).

$$\phi_i^{load} = cm_i^h \left(T_{g,i} - T_{hg,i}\right) \tag{14}$$

where ϕ_i^{load} represents the magnitude of the heat load at the node i, m_i^h represents the water supply flow of the heat load at the node i, $T_{g,i}$ and $T_{hg,i}$ represent the water supply temperature and the return water temperature at the node i respectively.

The thermal delay cannot be reflected in the heat balance relationship, but the delay time needs to be considered in the actual simulation calculation. The flow time of the liquid in the tube is approximately equal to the delay time of the heating network [28]. The flow time of hot water in the pipe section of the heating network with length Δ_l is shown as equation (15).

$$\Delta t = \frac{\Delta l \cdot \pi d^2 \rho}{4G_{g,t}} \tag{15}$$

where ρ is the density of the fluid, kg/m^3, Δl is the length of the pipe section, m, d is the inner diameter of the pipe section, m, $G_{g,t}$ is the fluid flow rate inside the pipe section at t, kg/h.

The distribution of the thermal power output by the EB is shown in equation (16) and the input, output power of the thermal storage tank satisfies equation (17).

$$H_{EB,i,t} = H_{EB,HL,i,t} + H_{EB,HS,i,t} \tag{16}$$

$$H_{EB,HS,i,t} = \lambda_{HS,IN} H_{HS,IN,i,t} \tag{17}$$

where $H_{EB,i,t}$ is the thermal output by the electric boiler of the i-th heating system, $H_{EB,HS,i,t}$ is the thermal output by the electric boiler to the heat storage tank of the i-th heating system, $H_{HS,IN,i,t}$ is the heat storage power of the heat storage

tank of the i-th heating system, $\lambda_{HS,IN}$ is the efficiency of the thermal tank device.

IV. ANALYSIS OF ENERGY STORAGE SITUATION DIVISION STRATEGY

The start-stop strategy of energy storage system is mainly divided into threshold start-stop and wind curtailment start-stop. In the threshold start-stop strategy, although reducing the threshold can improve the wind power accommodation rate, there also is a problem of starting energy storage when the heat load is high or without wind curtailment. It is clearly uneconomical because the process of produce thermal of electric boilers needs to consume high-grade electric energy while the thermal energy is low-grade energy relatively. Compared with the direct coal combustion for thermal, the efficiency of heating using high-grade electric energy is lower due to the addition of multiple energy conversions in the process [29]–[31]. The wind curtailment start-stop strategy can avoid unnecessary multiple energy conversions. Energy storage starts working during periods of high heat load and wind power curtailment, which is equivalent to converting excess wind power into thermal. The peak period of the electric load is shifted, while the accommodation rate of wind power and the operation economy of the system are improved.

A. BASIS AND PRINCIPLES OF ENERGY STORAGE SITUATION DIVISION

The basis of energy storage situation division: The energy storage system situation division method is proposed by imitating the different operating states of power systems and equipment under different operating conditions. For meeting the load demand, minimizing wind curtailment power and the economic cost, the energy storage system is divided into the following states: 1) electric boiler direct thermal state, 2) thermal storage tank state, 3) storage batteries state, 4) energy release state of the storage batteries and thermal storage tank.

The principle of energy storage situation division: The energy storage system adopts the wind curtailment start-stop plan. And according to the wind curtailment boundary power, the energy storage equipment is turned on to participate in regulation during the optimization process. To make the scheme feasible, it is necessary to judge whether the system has wind curtailment during the period time, which need to consider the electrical load of the system and the output of each set. If there have wind curtailment, the energy storage system is activated to participate in peak load regulating. Otherwise, the energy storage system releases energy to participate in heating.

B. ENERGY STORAGE SYSTEM ON-OFF JUDGEMENT MARK

The connection between the electric grid and the heating network are CHP units, EBs and non-power generation components (such as circulating pumps). The electrical power is produced by thermal power units, CHP units and wind power units. However, due to the constraints of heat load, the output regulation capacity of CHP units is greatly reduced. In addition, the reverse peak regulation and instability of wind power make peak regulation difficult, all tasks fall on the thermal power units. The time-shifting energy storage system has an important effect on the flexibility of the system and the accommodation of wind power. In the optimization process, when there have excess wind power in the system, the energy storage system participates in peak shaving according to the specific situation. Otherwise, the energy storage system releases energy according to the situation. The wind curtailment boundary power is the new definition proposed in this paper. Wind curtailment boundary power indicates the minimum boundary power value without wind curtailment, which is the minimum power output of the set without wind curtailment. The system's wind curtailment start-stop plan can not only reduce the wind curtailment volume, but also reduce the system operating cost. The wind curtailment boundary power is shown as equation (18).

$$P_{flag,i,t} = P_{CHP,\min,i,t} + P_{G,\min,t} + P_{PRW,t} \tag{18}$$

where $P_{flag,i,t}$ is the wind curtailment boundary power of the i-th heating system, $P_{CHP,\min,i,t}$ is the total minimum electric output of CHP unit of the i-th heating system, $P_{G,\min,t}$ is the minimum electric output of thermal power unit, $P_{PRW,t}$ is the predicted output of wind power.

C. JUDGEMENT OF ENERGY STORAGE SYSTEM SITUATION

Based on the relationship between the wind curtailment boundary power and the set output, energy storage capacity, the energy storage system is divided into four situations as follows.

1) ELECTRIC BOILER DIRECT THERMAL STATE

In the direct thermal control state of the electric boiler, the system electric load is provided by the thermal power units, CHP units and part of the output of wind turbines. The system heat load is provided by the CHP units and the part of wind power converted by electric boilers. The system wind curtailment boundary power and balance equation are shown as equation (19).

$$\begin{cases} P_{EL,t} < P_{flag,i,t} \le P_{EL,t} + \zeta_{EB} P_{EB,i,E} \\ H_{EV,i,t} = H_{CHP,i,t} + H_{EB,i,t} \\ P_{EL,t} = \sum_{i=1}^{M} P_{CHP,i,t} + P_{G,t} + P_{W,EL,t} \\ P_{W,t} = \sum_{i=1}^{M} P_{EB,i,t} + P_{W,EL,t} \\ H_{EB,i,t} = P_{EB,i,t}\eta_{EB} \\ 0 \le \zeta_{EB} \le 1 \end{cases} \tag{19}$$

where $P_{EB,i,E}$ is the rated electric power of the electric boiler of the i-th heating system, η_{EB} is the electric heating efficiency of the electric boiler, ζ_{EB} is the power utilization factor of the electric boiler.

2) THERMAL STORAGE TANK STATE

In the thermal storage state of the thermal storage tank, the electrical load of the system is provided by the thermal power units, CHP units and part of the output of wind turbines. The system heat load is provided by the CHP units and the part of wind power converted by electric boilers (note that the thermal storage tank only stores energy at this time). The system wind curtailment boundary power and balance equation are shown as equation (20).

$$\begin{cases} P_{EL,t} + \zeta_{EB} P_{EB,i,E} < P_{flag,i,t} \le P_{EL,t} + P_{EB,i,E} \\ H_{EV,i,t} = H_{CHP,i,t} + H_{EB,i,t} \\ P_{EL,t} = \sum_{i=1}^{M} P_{CHP,i,t} + P_{G,t} + P_{W,EL,t} \\ P_{W,t} = \sum_{i=1}^{M} P_{EB,i,t} + P_{W,EL,t} \\ H_{EB,i,t} = \zeta_{EB} P_{EB,i,E} \eta_{EB} \\ H_{HS,IN,i,t} = (P_{EB,i,t} - \zeta_{EB} P_{EB,i,E}) \eta_{EB} \\ S_{HS,i,t} = (1-\mu) S_{HS,i,t-1} + H_{HS,IN,i,t} \lambda_{HS,IN} \end{cases} \tag{20}$$

where $S_{HS,i,t}$ is the heat storage capacity of the heat storage tank of the i-th heating system, μ is the thermal loss rate of the heat storage tank.

3) STORAGE BATTERIES STATE

In the state of storage batteries, the electrical load of the system is provided by the thermal power units, CHP units and part of the output of wind turbines. The heat load of the system is provided by CHP units and the part of wind power converted by electric boilers. The system wind curtailment boundary power and balance equation are shown as equation (21).

$$\begin{cases} P_{EL,t} + P_{EB,i,E} < P_{flag,i,t} \\ H_{EV,i,t} = H_{CHP,i,t} + H_{EB,i,t} \\ P_{EL,t} = \sum_{i=1}^{M} P_{CHP,i,t} + P_{G,t} + P_{W,EL,t} \\ P_{W,t} = \sum_{i=1}^{M} P_{EB,i,t} + P_{W,EL,t} + P_{EES,CHA,t} \\ H_{EB,i,t} = \zeta_{EB} P_{EB,i,E} \eta_{EB} \\ H_{HS,IN,i,t} = (P_{EB,i,t} - \zeta_{EB} P_{EB,i,E}) \eta_{EB} \\ S_{HS,i,t} = (1-\mu) S_{HS,i,t-1} + H_{HS,IN,i,t} \lambda_{HS,IN} \\ E_{EES,t} = (1-\tau) E_{EES,t-1} + P_{EES,CHA,t} \gamma_{EES,CHA} \end{cases} \tag{21}$$

where $E_{EES,t}$ is the storage capacity of the storage batteries device, MWh, τ is the self-loss rate of the electric power of the storage batteries device, $\gamma_{EES,CHA}$ is the charging efficiency of the storage batteries device.

4) ENERGY RELEASE STATE OF THE STORAGE BATTERIES AND THERMAL STORAGE TANK

When the energy storage system is in the release state of the storage batteries and thermal storage tank, the electrical load of the system is provided by electrical energy storage and thermal power units, CHP units and all output of wind turbines. The system heat load is provided by CHP units and thermal storage tanks. The system wind curtailment boundary power and balance equation are shown as equation (22).

$$\begin{cases} P_{flag,i,t} \le P_{EL,t} \\ S_{HS,i,t} = (1-\mu) S_{HS,i,t-1} - \dfrac{H_{HS,OUT,i,t}}{\lambda_{HS,OUT}} \\ E_{EES,t} = (1-\tau) E_{EES,t-1} - \dfrac{P_{EES,DIS,t}}{\gamma_{EES,DIS}} \\ H_{EV,i,t} = H_{CHP,i,t} + H_{HS,OUT,i,t} \\ P_{EL,t} = \sum_{i=1}^{M} P_{CHP,i,t} + P_{G,t} + P_{W,t} + P_{EES,DIS,t} \end{cases} \tag{22}$$

where $\lambda_{HS,out}$ is the release efficiency of the heat storage tank.

The energy storage system situation division strategy is shown in Figure 2. The specific process is shown as follows.

① Under the premise of the minimum electric output of the thermal power units and the CHP units, the system has surplus wind power, the wind curtailment boundary power is more than the system electrical load. At this time, the electric boiler starts to work and the surplus wind power is converted into thermal power by the electric boiler. The thermal energy of the system is directly supplied by the electric boiler, while the CHP unit reduces the thermal output.

② Under the premise of the minimum electric output of the thermal power units and CHP units, the system has surplus wind power, the wind curtailment boundary power is more than the sum of the system electrical load and the rated power

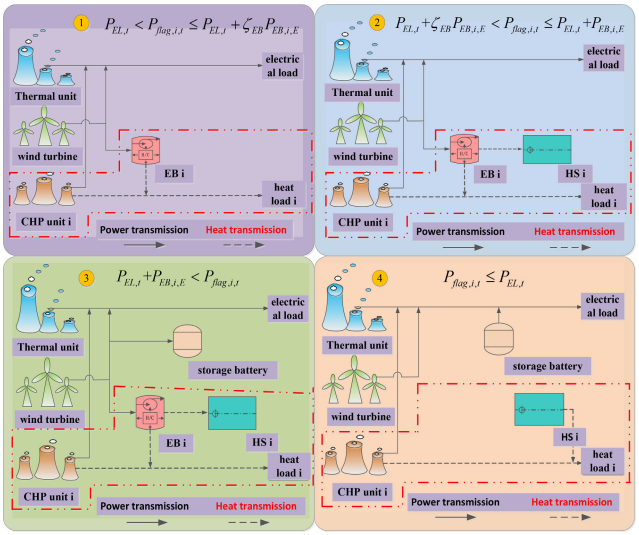

FIGURE 2. Energy storage system regulation strategy diagram.

of some electric boilers. The heat storage tank is activated, the excess wind power is converted into heat energy and stored in the heat storage tank.

③ When the electric boiler is operating at the rated power, the energy storage system is in the storage batteries state. The remaining wind power that does not exceed the rated electric power of the electric boiler is converted into heat power by the electric boiler to supply the heat load and the heat storage tank. Part of the electric power which exceeds the rated electric power of the electric boiler is supplied to storage batteries.

④ When the wind curtailment boundary power is less than the electrical load of the system, all the wind power output is used to supply the electrical load, the thermal power unit and CHP unit increase the electrical output to ensure the balance of power supply and demand. At this time, the storage batteries and the thermal storage tank have stored energy. The thermal storage tank can directly release thermal to the heating network and the storage batteries can release electrical energy to the electric load.

Note that the energy storage system regulation strategy diagram corresponds to the model in Figure 1, which includes only one electric power system and multiple thermal systems. The storage batteries of electric power system in Figure 2 are used as a whole unit and the final optimization result of which can be obtained comprehensively.

V. MULTI-OBJECTIVE OPTIMIZATION MODEL OF INTEGRATED ELECTRIC-HEAT SYSTEM BASED ON ENERGY STORAGE SITUATION DIVISION

This paper comprehensively considers the transmission characteristics of the integrated network and the coordination of flexible resources such as electric boilers, thermal storage tanks and storage batteries. A dual-objective optimization model with the minimum operating cost of the system and the minimum wind curtailment volume is established.

A. OBJECTIVE FUNCTION

1) OBJECTIVE FUNCTION 1

The objective function of the minimum wind curtailment volume of the dispatching system is shown as equation (23).

$$\min f_K = \sum_{t=1}^{T} (P_{W,t} - P_{PW,t}) \tag{23}$$

where f_K is wind curtailment power of dispatching system, $P_{PW,t}$ is the actual output of the wind turbine.

2) OBJECTIVE FUNCTION 2

The value of wind curtailment is also the economic loss of the system, so the objective function of the smallest operating cost of system is shown as equation (24).

$$\min f_P = \sum_{t=1}^{T} (C_{G,t} + C_{CHP,t} - C_W(P_{W,t} - P_{PW,t})) \tag{24}$$

where f_P is the total operating cost of the system, \$, C_G is the operating cost of the thermal power unit, \$, C_{CHP} is the operating cost of the CHP units of the i-th heating system, \$, C_W is the price of wind power, \$/MW.

The operating cost of the CHP unit is shown as equation (25) [32].

$$C_{CHP,t} = \sum_{i=1}^{M} \begin{aligned}(&A_i P_{CHP,i,t}^2 + B_i P_{CHP,i,t} + C_i P_{CHP,i,t} H_{CHP,i,t} \\ &+ D_i H_{CHP,i,t}^2 + E_i H_{CHP,i,t} + F_i)\end{aligned} \tag{25}$$

where $A_i \sim F_i$ is the cost coefficient of the i-th CHP unit.

The operating cost of the thermal power unit is shown as equation (26) [33].

$$C_{G,t} = \sum_{j=1}^{N} (a_j P_{G,j,t}^2 + b_j P_{G,j,t} + c_j) \tag{26}$$

where$a_j \sim c_j$ is the cost coefficient of the j-th thermal power unit.

3) COMPREHENSIVE OPTIMIZATION GOAL

Taking into account the different dimensions of two objective functions, multi-objective optimization is transformed into single-objective optimization. The objective function is transformed into the greatest satisfaction within the constraints, which is shown as equation (27).

$$\mu_{\max} = k_1 \mu_K + k_2 \mu_P \tag{27}$$

where k_1 and k_2 are the weight coefficients, satisfying $k_1 + k_2 = 1$. The two membership functions are shown in equation (28) and (29).

$$\mu_K = \begin{cases} 0 & f_K < K_{\max} - \delta_1 \\ \dfrac{f_K - (K_{\max} - \delta_1)}{\delta_1} & K_{\max} - \delta_1 \le f_K \le K_{\max} \\ 1 & f_K > K_{\max} \end{cases} \tag{28}$$

$$\mu_P = \begin{cases} 1 & f_P < P_{\min} \\ \dfrac{P_{\min} + \delta_2 - f_P}{\delta_2} & P_{\min} \le f_P \le P_{\min} + \delta_2 \\ 0 & f_P > P_{\min} + \delta_2 \end{cases} \tag{29}$$

where μ_K is the membership function of the wind power accommodation, μ_P is the membership function of the total system operating cost, f_K and f_P respectively correspond to the specific values of $\max f_k$ and $\min f_p$ in each optimization period, $K_{\max}$ is the specific function value when the maximum wind power accommodation is the target, $P_{\min}$ is the specific function value when the minimum total operating cost is the target, δ_1 is the acceptable expansion value when the wind power accommodation is the maximum, δ_2 is the acceptable expansion value when the total operating cost is the minimum.

The membership function of the two goals is shown in Figure 3.

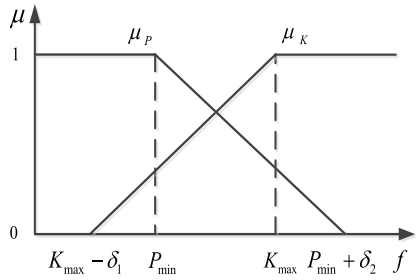

FIGURE 3. The membership function of the two targets.

B. RESTRICTIONS

1) POWER FLOW CONSTRAINT EQUATION

The power flow constraints are shown as equation (30) [27]:

$$\begin{cases} P_i = U_i \sum_{j\in i} U_j(G_{ij}\cos\theta_{ij} + B_{ij}\sin\theta_{ij}) \\ Q_i = U_i \sum_{j\in i} U_j(G_{ij}\sin\theta_{ij} - B_{ij}\cos\theta_{ij}) \\ -P_i^{\max} \le P_i \le P_i^{\max} \\ -Q_i^{\max} \le Q_i \le Q_i^{\max} \end{cases} \tag{30}$$

where P_i and Q_i are the active and reactive power injections at node i. $P_i^{\max}$ and $Q_i^{\max}$ are the allowable active limit transmission power and reactive limit transmission power of branch i, respectively. U_i and U_j are the voltage amplitudes of nodes i and j. G_{ij} and B_{ij} are the conductance and susceptance of branch ij. θ_{ij} is the voltage phase angle difference between the i-th and$j$-th node.

2) OPERATIONAL CONSTRAINTS OF STORAGE BATTERIES SYSTEM

The constraints of storage batteries are divided into state of charge constraints, maximum charge and discharge power constraints, which are shown as equation (31).

$$\begin{cases} E_{EES,t+1} = E_{EES,t} + P_{EES,CHA,t}\gamma_{EES,CHA}T \\ \qquad\qquad - \dfrac{P_{EES,DIS,t}T}{\gamma_{EES,DIS}} \\ E_{EES,\max} \times 20\% \le E_{EES,t+1} \le E_{EES,\max} \times 90\% \\ E_{EES,\max} \times 20\% \le E_{EES,t} \le E_{EES,\max} \times 90\% \\ 0 \le P_{EES,CHA,t} \le D_{CHA,t}P_{EES,\max,t}^{CHA} \\ 0 \le P_{EES,DIS,t} \le D_{DIS,t}P_{EES,\max,t}^{DIS} \end{cases} \tag{31}$$

where $E_{EES,t+1}$ is the remaining capacity of the storage batteries device at the end of the $t+1$ cycle, $P_{EES,CHA,t}$ and $P_{EES,DIS,t}$ are the charge and discharge power of the system, $\gamma_{EES,CHA}$, $\gamma_{EES,DIS}$ are the charge and discharge efficiency of the system, $E_{EES,\max}$ is the maximum capacity of the battery in stable operation, $P_{EES,\max,t}^{CHA}$ and $P_{EES,\max,t}^{DIS}$ are the maximum charge and discharge power of storage batteries. $D_{CHA,t}$, $D_{DIS,t}$ and $D_{NW,t}$ are the charge, discharge and downtime states of storage batteries. It only can be one state at a certain moment, which is 0, −1 or 1.

3) OPERATIONAL CONSTRAINTS OF REGENERATIVE ELECTRIC BOILERS

The capacity of the electric boiler is limited to a certain extent and its operating electric power has upper and lower limits, which will cause damage to the electric boiler when it crosses the boundary. The power constraint of the electric boiler can be shown as equation (32).

$$0 \le P_{EB,t} \le P_{EB,\max,t} \tag{32}$$

where $P_{EB,\max,t}$ is the upper power limit of electric boiler.

As an energy storage device, the thermal storage tank needs to maintain a balance of capacity. It only can be one state, which is heat release or heat storage. The constraint conditions of the thermal storage tank is shown as equation (33).

$$\begin{cases} S_{HS,\min} \le S_{HS,t} \le S_{HS,\max} \\ H_{HS,\min} \le H_{HS,OUT,i,t} \le H_{HS,\max} \\ S_{OH,\min} \le S_{OH,t} \le S_{OH,\max} \end{cases} \tag{33}$$

where $S_{HS,\min}$ and $S_{HS,\max}$ are the minimum and maximum capacities of the heat storage tank under stable operation conditions, $H_{HS,\min}$ and $H_{HS,\max}$ are the minimum and maximum values of output power, $S_{OH,\min}$ and $S_{OH,\max}$ are the minimum and maximum values of heat storage and residual heat state. Also, it only can be one state at a certain moment, which is thermal storage or thermal release.

4) OUTPUT CONSTRAINTS OF THERMAL POWER UNITS

The electric output constraint of thermal power unit is shown as equation (34).

$$P_{G,j,\min} \le P_{G,j,t} \le P_{G,j,\max} \tag{34}$$

where $P_{G,j,\min}$ and $P_{G,j,\max}$ are the lower limit and upper limit of the electric power of the j-th thermal power unit.

5) WIND TURBINE OUTPUT CONSTRAINTS

The output of wind turbine is more difficult to predict. It is affected by the magnitude of the wind power and has high volatility and randomness. We can see Appendix A for wind power forecasting methods. During the optimization process, the output of wind turbines cannot exceed the predicted value. The output constraints of wind turbines are shown as equation (35).

$$0 \le P_{W,t} \le P_{PRW,\max,t} \tag{35}$$

where $P_{PRW,\max,t}$ is the predicted output of the wind turbine.

6) CONSTRAINTS OF THE THERMAL-ELECTRIC OPERATIONAL DOMAIN OF CHP UNIT

When the system is running, the CHP units need to meet the constraints of the thermal-electric operational domain, which

is shown as equation (36).

$$\begin{cases} H^{\min}_{CHP,i,t}(P_{CHP,i,t}) \le H_{CHP,i,t} \le H^{\max}_{CHP,i,t}(P_{CHP,i,t}) \\ P^{\min}_{CHP,i,t}(H_{CHP,i,t}) \le P_{CHP,i,t} \le P^{\max}_{CHP,i,t}(H_{CHP,i,t}) \end{cases} \tag{36}$$

where $H^{\min}_{CHP,i,t}(P_{CHP,i,t})$, $H^{\max}_{CHP,i,t}(P_{CHP,i,t})$, $P^{\min}_{CHP,i,t}(H_{ChP,i,t})$ and $P^{\max}_{CHP,i,t}(H_{CHP,i,t})$ form a linear inequality to determine the thermoelectric operational domain (FOR) of the CHP unit. The mathematical expression of FOR is shown as equation (37).

$$b_{m\,i}H_{CHP,i,t} + c_{m\,i}P_{CHP,i,t} \ge d_{m\,i} \quad m = 1, 2, 3 \tag{37}$$

where b_{mi}, c_{mi} and d_{mi} represent the coefficients of the FOR inequality of the i-th CHP unit.

7) CONSTRAINTS OF POWER GRID BRANCH

The transmission line of power grid needs to meet the capacity constraint, which is shown as equation (38) [34].

$$P_d^{line\,\min} \le P_{d,t}^{line} \le P_d^{line\,\max} \tag{38}$$

where $P_{d,\mathrm{t}}^{line}$ represents the transmission power of the grid branch d, $P_d^{line\ \min}$ and $P_d^{line\ \max}$ represent the upper and lower limits of the transmission power of the grid branch d Respectively.

8) CONSTRAINTS OF THE HEATING NETWORK BRANCH

The transmission pipeline of the heating network also needs to meet the branch constraints, which are shown as equation (39) [1].

$$\begin{aligned} T_g^{\min} &\le T_{g,t} \le T_g^{\max} \\ m_g^{\min} &\le m_{g,t} \le m_g^{\max} \\ q_{g,t} &= cm_{g,t}(T_{g,t} - T_{hg,t}) \end{aligned} \tag{39}$$

where $T_g^{\max}$ and $T_g^{\min}$ are the upper and lower limits of the water supply temperature in pipe g of the heating network. $m_{g,t}$ is the flow, $m_g^{\min}$ and $m_g^{\max}$ are the upper and lower limits, m^3/h, $q_{g,t}$ is the transfer heat, $T_{hg,t}$ is the return water temperature.

VI. OPTIMAL SCHEDULING STRATEGY BASED ON DOUBLE λ ITERATIVE ALGORITHM

To effectively solve the integrated electric-heat system model that takes into account the smallest operating cost of system and the smallest wind curtailment volume, this paper designs a double λ iterative algorithm for optimization calculations. According to the output coordination relationship of each set of the system, the integrated electric-heat system is divided into the power subsystem λ_P iteration and heating subsystem λ_h iteration, so the power subsystem does not need to provide power grid topology parameters, operating costs parameters, electrical load demand parameters and wind forecast power to the heating subsystem. Similarly, the heating subsystem does not need to provide heating network topology parameters, operating cost parameters and heat load demand parameters to the power subsystem. It can effectively reduce the information interaction, the calculation and communication burden so that the algorithm converges quickly while protecting the privacy of the subsystems.

The CHP unit and electric boiler as the link between the electric power subsystem and the heating subsystem, which perform double λ iteration to achieve information interaction and resource coordination configuration. Through the repeated iterative solution, the double Lagrange multiplier and unit output are continuously modified. And finally, the optimal solution is obtained when the system power deviation meets the convergence condition. The flow chart of the multi-objective optimization model in this paper is shown in Figure 4.

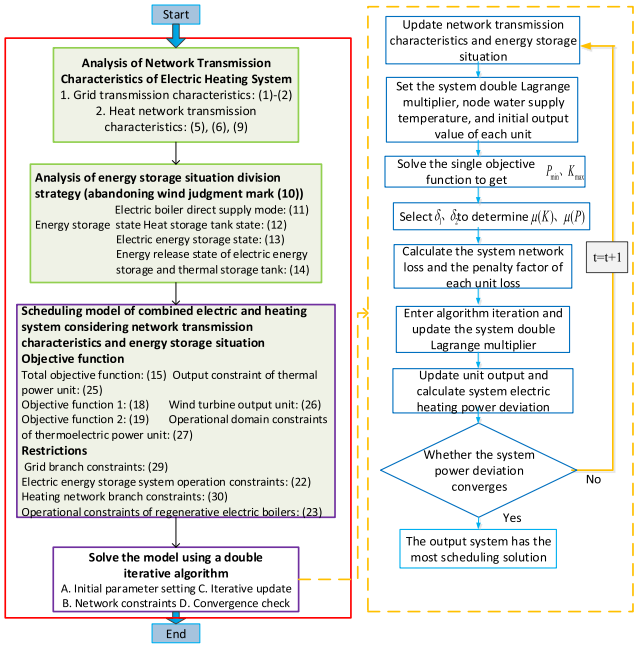

FIGURE 4. Flow chart of the multi-objective optimization model.

A. INITIAL PARAMETER SETTING

Set the initial output value of each unit when t = 0, which is shown as equation (40).

$$\begin{cases} \sum_{i=1}^{M} P_{CHP,i,0} + P_{G,0} + P_{EES,DIS,0} + P_{W,EL,0} \\ -P_{EES,CHA,0} - \sum_{i=1}^{M} P_{EB,i,0} - P_{EL,0} = 0 \\ \sum_{i=1}^{M} (H_{CHP,i,0} + H_{EB,HL,i,0} + H_{HS,OUT,i,0} - H_{EV,i,0}) = 0. \end{cases} \tag{40}$$

The initial value $\lambda_{P,0}$ and $\lambda_{h,0}$ of the double Lagrange multiplier, and the initial value $T_{g,0}$ of the system are set.

B. NETWORK CONSTRAINTS

Firstly, the unit's power output should meet the branch power flow constraints, which are shown as equation (41) and (42).

$$\begin{cases} Q_{r,t} = Q_{r,t}\ , P_d^{line\ \min} \le Q_{r,t}\ \le P_d^{line\ \max} \\ Q_{r,t} = P_d^{line\ \max}\ ,\ Q_{r,t} \ge P_d^{line\ \max} \end{cases} \tag{41}$$

$$\begin{cases} P_{CHP,i,t} = P_{CHP,i,t}\ ,\ P_d^{line\ \min} \le P_{CHP,i,t}\ \le P_d^{line\ \max} \\ P_{CHP,i,t} = P_d^{line\ \max}\ ,\ P_{CHP,i,t} \ge P_d^{line\ \max} \end{cases} \tag{42}$$

Secondly, the water supply temperature of the heating network pipeline should meet the branch constraints, which is shown as equation (43).

$$\begin{cases} T_{g,t} = T_{g,t}, T_g^{\min} < T_{g,t}\ < T_g^{\max} \\ T_{g,t} = T_g^{\min}\ , T_{g,t} \le T_g^{\min} \\ T_{g,t} = T_g^{\max}\ , T_{g,t} \ge T_g^{\max} \end{cases} \tag{43}$$

Thirdly, the pipe flow of the heating network should meet the branch constraints, which are shown as equation (44) and (45).

$$m_{g,t} = \frac{q_{g,t}}{c(T_{g,t} - T_{hg,t})} \tag{44}$$

$$\begin{cases} m_{g,t} = m_{g,t}, m_g^{\min} < m_{g,t} < m_g^{\max} \\ m_{g,t} = m_g^{\min},\ m_{g,t} \le m_g^{\min} \\ m_{g,t} = m_g^{\max}, m_{g,t} \ge m_g^{\max} \end{cases} \tag{45}$$

Finally, update the heat transfer of the heating network node as equation (46).

$$\begin{cases} q_{g,t} = cm_{g,t}(T_{g,t} - T_{hg,t}) \\ H_{CHP,i,t} = q_{g,t}\ , H_{CHP,i,t} \ge q_{g,t} \end{cases} \tag{46}$$

C. ITERATIVE UPDATE

According to equation (47)-(49), the loss penalty factor corresponding to each suite is calculated as follows.

$$pf_{Or,t} = \frac{1}{(1 - 2(\sum_{m=1}^{R} B_{rm}O_{m,t} + \sum_{i=1}^{M} B_{ri}P_{i,t}))} \tag{47}$$

$$pf_{ci,t} = \frac{1}{(1 - \sum_{n=1}^{M} B_{in}P_{n,t} - 2\sum_{r=1}^{R} B_{ri}O_{r,t})} \tag{48}$$

$$hf_{ci,t} = \frac{1}{(1 - \frac{2\pi l_g}{cm_{g,t}\sum R})} \tag{49}$$

Let Ω_p denote the collection of pure generator units whose electric output reaches the upper or lower limit, let Ω_{co} denote the collection of CHP units whose electric output reaches the boundary of the operational domain, let Ω_{ch} denote the collection of CHP units whose thermal output reaches the boundary of the operational domain.

According to equation (50) and (51), update the system double Lagrange multiplier as follows.

$$\begin{aligned} \lambda_{p,t+1} = (&\sum_{l=1}^{L} P_{EL,l,t} + P_{E,t} - \sum_{r\in\Omega_p} O_{r,t} - \sum_{i\in\Omega_{co}} H_{CHP,i,t} \\ &+ \sum_{j\notin\Omega_p} \frac{b_j}{2a_j} + \sum_{i\notin\Omega_{co}} \frac{B_i + C_i P_{CHP,i,t}}{A_i}) \\ &/(\sum_{j\notin\Omega_p} \frac{1}{2a_j pf_{Or,t}} + \sum_{i\notin\Omega_{co}} \frac{1}{A_i pf_{ci,t}}) \end{aligned} \tag{50}$$

$$\begin{aligned} \lambda_{h,t+1} = (&\sum_{v=1}^{V} H_{EV,v,t} + H_{E,t} \\ &- \sum_{i\in\Omega_{ch}} P_{CHP,i,t} + \sum_{i\notin\Omega_{ch}} \frac{E_i + C_i H_{CHP,i,t}}{2D_i}) \\ &/ \sum_{i\notin\Omega_{ch}} \frac{1}{2D_i hf_{ci,t}} \end{aligned} \tag{51}$$

Furthermore, the temperature of the water supply and transmission flow of pipeline are updated by equation (52)-(53), also the dispatching output of each suite is updated by equation (54)-(56).

$$T_{g,t+1} = \frac{q_{g,t+1}}{cm_{g,t}} + T_{hg,t} \tag{52}$$

$$m_{g,t+1} = \frac{q_{g,t+1}}{c(T_{g,t+1} - T_{hg,t+1})} \tag{53}$$

$$H_{CHP,i,t+1} = \begin{cases} \frac{1}{pf_{ci}2A_i}\lambda_{p,t+1} - \frac{C_i}{2A_i} \\ P_{CHP,i,t} - \frac{B_i}{2A_i}\ , \forall i \notin \Omega_{co} \\ H_{CHP,i}^{\min}(P_{CHP,i,t})\ or \\ H_{CHP,i}^{\max}(P_{CHP,i,t}),\ \forall i \in \Omega_{co} \end{cases} \tag{54}$$

$$O_{r,t+1} = \begin{cases} \frac{1}{pf_{or}2a_j}\lambda_{p,t+1} - \frac{b_j}{2a_j}\ , \forall r \notin \Omega_p \\ O_r^{\min}\ or\ O_r^{\max}\ ,\ \forall r \in \Omega_p \end{cases} \tag{55}$$

$$P_{CHP,i,t+1} = \begin{cases} \frac{1}{hf_{ci,t}2D_i}\lambda_{h,t+1} - \frac{C_i}{2D_i} \\ H_{CHP,i,t+1} - \frac{E_i}{2D_i}, \forall i \notin \Omega_{ch} \\ P_{CHP,i}^{\min}(H_{CHP,i,t+1})\ or \\ P_{CHP,i}^{\max}(H_{CHP,i,t+1}), \forall i \in \Omega_{ch} \end{cases} \tag{56}$$

D. CONVERGENCE CHECK

The system electric power deviation and system thermal deviation are shown as equation (57) and (58).

$$\begin{aligned} \Delta P_{t+1} = (&\sum_{r=1}^{R} O_{r,t+1} + \sum_{i=1}^{M} P_{CHP,i,t+1} + P_{EES,DIS,t+1} \\ &- P_{EES,CHA,t+1} - \sum_{i=1}^{M} P_{EB,i,t} - \sum_{l=1}^{L} P_{EL,l,t+1} \\ &- P_{E,t}) \end{aligned} \tag{57}$$

$$\Delta H_{t+1} = \sum_{i=1}^{M}(H_{CHP,i,t+1} + H_{EB,HL,i,t+1} + H_{HS,OUT,i,t+1} - H_{EV,i,t+1} - H_{E,i,t}) \quad (58)$$

The convergence condition is set as equation (59) to determine whether the system power deviation meets the convergence condition, if not, repeat the update. Otherwise, output the current optimal output of each set.

$$\max \begin{cases} |\Delta P_{t+1}| \\ |\Delta H_{t+1}| \end{cases} \leq \xi \quad (59)$$

where ξ represents the convergence determination coefficient, which is generally 10^{-3}.

VII. CASE ANALYSIS

A. CASE SYSTEM

The structure diagram of the simulation system is shown in Figure 5. The system consists of one standard 14-nodes power system and two 10-nodes heating system [1], they are real measured values.

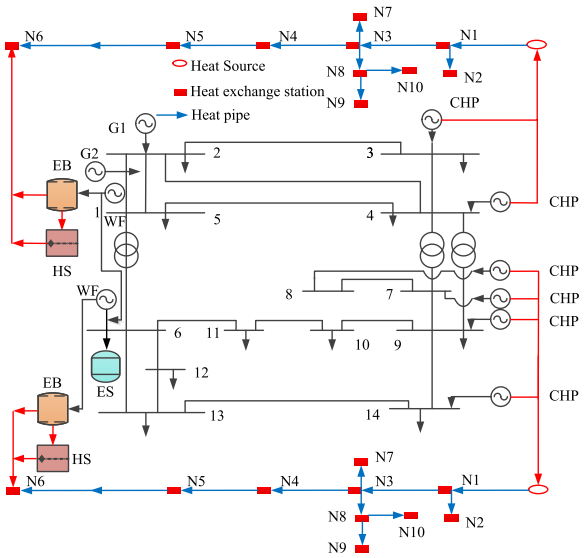

FIGURE 5. Simulation system structure diagram.

The detailed parameters setting for the energy storage system, power network and heating network are shown in Appendix B. In this paper, the heat load of heating network 2 is proportional to the heat load of heating network 1. Specifically, N1-N5 is 1.3-fold relationship, while N6-N10 is 0.8-fold relationship. The wind power forecasting process is shown in Appendix A. The generator units $G_{r1} \sim G_{r4}$ includes two thermal power units and two wind turbines, corresponding to nodes 1, 2, 5 and 6. The CHP units $G_{c1} \sim G_{c6}$ correspond to nodes 3, 4, 7, 8, 9, 14. The electrical load demand and heat load demand of the system refer to the electrical and heat load of node 13. It is assumed that there are three communities in the vicinity of node 13. For the convenience of calculation, the residential buildings in each community are simplified into row residential buildings. Set the convergence determination coefficient $\xi = 10^{-3}$, the network loss coefficient matrix B is shown as follows.

$$B = \begin{bmatrix} 11 & 5 & 7 & 5 & 5 & 6 & 5 & 4 & 3 & 4 \\ 5 & 12 & 3 & 6 & 5 & 7 & 5 & 2 & 2 & 6 \\ 7 & 3 & 13 & 4 & 2 & 5 & 5 & 7 & 6 & 5 \\ 5 & 6 & 4 & 14 & 4 & 6 & 5 & 3 & 4 & 6 \\ 5 & 5 & 2 & 4 & 15 & 3 & 5 & 6 & 7 & 4 \\ 6 & 7 & 5 & 6 & 3 & 11 & 6 & 5 & 6 & 3 \\ 5 & 5 & 5 & 5 & 5 & 6 & 12 & 4 & 5 & 4 \\ 4 & 2 & 7 & 3 & 6 & 5 & 4 & 13 & 6 & 5 \\ 3 & 2 & 6 & 4 & 7 & 6 & 5 & 6 & 14 & 3 \\ 3 & 5 & 3 & 6 & 3 & 6 & 7 & 2 & 6 & 12 \end{bmatrix} \times 10^{-6}$$

We set $T_0 = 0°$, which is the average temperature of the medium around the heat pipeline, we set $T_{hg} = 30°$C, which is the average temperature of water return, also we set the initial value of the water temperature of each node of the heating network, which is $T_{g,0} = 96°$C. The specific heating capacity of the heat medium is $c = 4.2 \times 10^3 KJ/(kg \cdot °\,\text{C})$, the price of wind power is 101.48$/MWh, the initial value of double Lagrange multiplier are set as $\lambda_{p,0} = 0.45$, $\lambda_{h1,0} = 0.5$ and $\lambda_{h2,0} = 0.5$.

B. SCHEDULING SIMULATION

This paper set three scenarios to analyze the impact of network transmission characteristics and energy storage situation on the operating cost of the system and wind power accommodation.

Scenario 1: Optimal dispatch of single heat source integrated electric-heat system (S1).

Scenario 2: Optimal dispatch of the integrated electric-heat system under the hierarchical regulation scheme of energy storage system without considering the network transmission characteristics (S2).

Scenario 3: Optimal dispatch of the integrated electric-heat system with energy storage considering network transmission characteristics (S3).

The comparison results of scenario 1 and scenario 2 can analyze the impact of the energy storage system on the integrated electric-heat system. Also, the comparison results of scenario 2 and scenario 3 can analyze the influence of network transmission characteristics on the electric-heat interconnection system. Here scenario 3 is the integrated electric-heat system model of this paper.

TABLE 1 shows the total system cost and the wind curtailment consumption volume of the three scenarios. Comparing scenario 3 with scenario 1, the total system cost and wind curtailment volume are reduced by 1.1062×10^3 $and 110MW respectively.

TABLE 2 shows the simulation time and effectiveness comparative analysis of the model under the conventional optimization algorithm [20], [21] and the double λ iterative algorithm. We compare the results of power deviation of double λ iterative algorithm with GA's, PSO's, mixed integer linear programmings, and the results are shown in Figure 6.

TABLE 1. The total system cost and the amount of wind curtailment under the three scenarios.

Scenes	Total system cost/10^3\$	Wind consumption/MW
1	8.3688	15
2	8.3671	40.6
3	7.2626	125

TABLE 2. Comparison and analysis of optimization algorithms.

	MILP A[21]	PSO [13]	GA[14]	Double λ iterative algorithm	Computer level
Simulation time (s)	65.89	59.65	50.283	30.5397	CPU: i5-5200U Memory: 12GB Hard Disk: SA400S37240G+240G
Simulation accuracy	77.45 %	75.9 %	80.6%	93.7%	

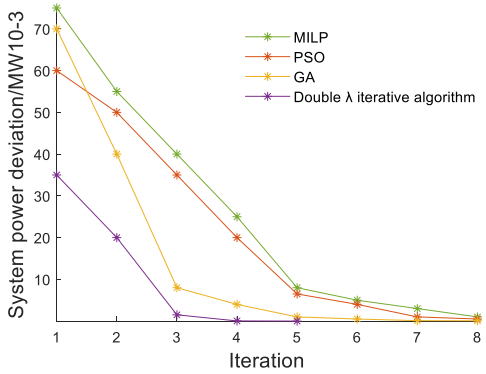

FIGURE 6. Algorithm convergence speed comparison.

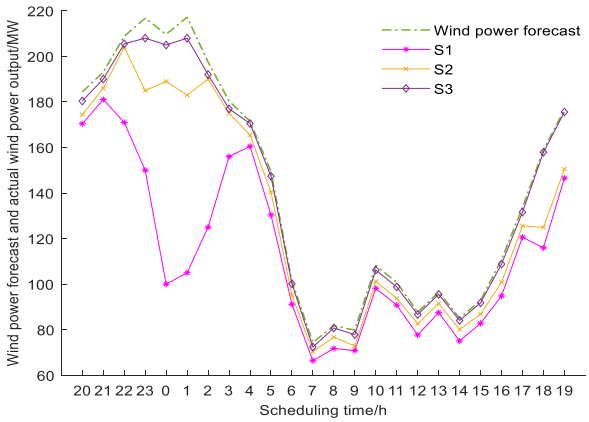

FIGURE 7. Total forecasted wind power and actual wind power output under different scenarios.

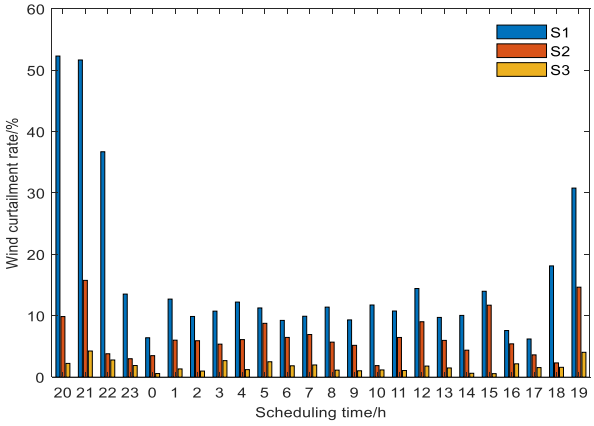

FIGURE 8. Wind curtailment rate under different scenarios.

Therefore, considering the simulation speed and simulation accuracy, the calculation example in this paper uses the double λ iterative algorithm to solve the calculation.

Furthermore, the forecast of wind power and the actual output of wind power, the total power output of the thermal power units and the CHP units under different scenarios and the total thermal output of the CHP units are shown in Figure 7-13.

C. ANALYSIS OF SCHEDULING RESULTS IN DIFFERENT SCENARIOS

1) ACTUAL WIND POWER OUTPUT AND SYSTEM OPERATING COST

Combined with Figure 7-8, it can be seen that the S1 scheme has the lowest on-grid of wind power, especially during periods of high wind power generation such as 18:00-23:00. The curtailment rate is as high as 22%∼50%, which severely restricts the accommodation of wind power and the system operating costs are also high. In S2, after adding energy storage resources to participate in the regulation, the wind power abandonment rate is significantly reduced. During the period from 19:00 to 21:00, the wind power abandonment rate is slightly higher, ranging from 10% to 16%. When the S3 dispatching scheme is adopted, the wind power accommodation actually is the maximum. Except for some high wind power generation periods, the wind power on-grid rate is above 96% in the rest of the period. The full accommodation of wind power is basically achieved. The energy utilization structure of the system is adjusted, which further reduces the operating costs overall system. At night, wind power output obviously exhibits reverse regulation characteristics. Due to the low electrical load at night and high heat load, energy storage systems are generally required to assist peak load regulating.

It can be seen from TABLE 1 that under the scenario of considering electric boilers, thermal storage tanks, and storage batteries, the operating cost of the system is increased, but the benefits brought by the accommodation of wind power in the integrated system are reduced the overall cost.

2) ELECTRIC AND THERMAL OUTPUT OF THE UNIT

It can be seen from Figure 8 that the power output of the units in different scenarios is roughly the same, but due to the similarities and differences between the network

TABLE 3. The delay time Δt and the thermal attenuation H_E are converted to each node.

Node	N_1^1	N_2^1	N_3^1	N_4^1	N_5^1	N_6^1	N_7^1	N_8^1	N_9^1	N_{10}^1
Delay time/h	1.09	0.67	1.04	1.29	2.06	2.28	2.04	1.22	2.11	2.18
Thermal decay/MWth	7.30	15.25	9.43	2.36	5.11	5.97	5.97	2.54	5.97	5.87
Node	N_1^2	N_2^2	N_3^2	N_4^2	N_5^2	N_6^2	N_7^2	N_8^2	N_9^2	N_{10}^2
Delay time/h	1.21	1.05	0.78	1.24	1.96	2.56	2.35	1.23	1.16	1.98
Thermal decay/MWth	6.30	16.23	10.25	3.63	4.23	6.32	6.32	3.2	5.66	5.89

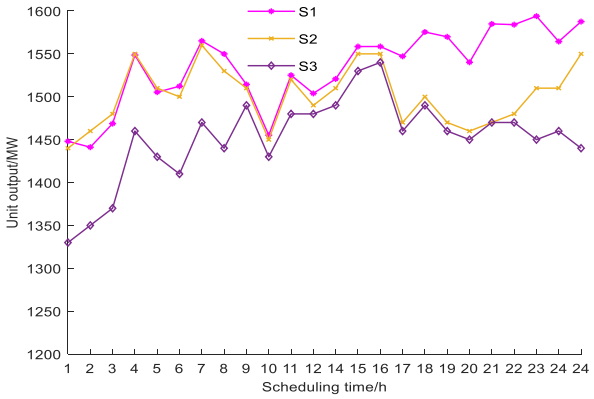

FIGURE 9. Comparison curves of unit electric output under different scenarios.

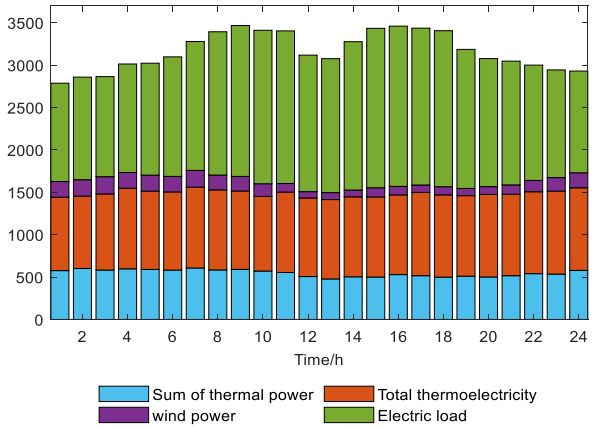

FIGURE 11. Electric output of each unit under S2.

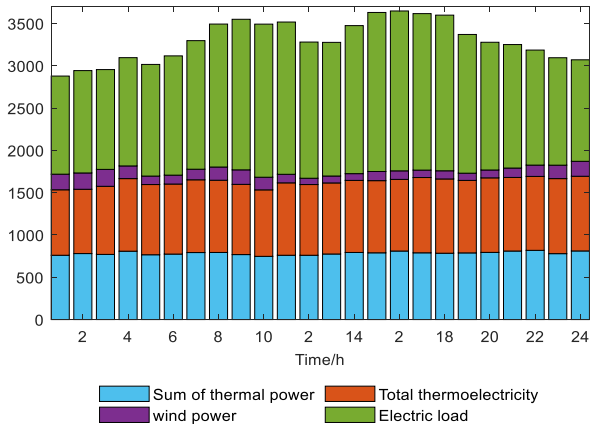

FIGURE 10. Electric output of each unit under S1.

characteristics and the hierarchical control strategy of energy storage, the power output of the units is slightly different. During the period 1-10, the power output of S1 and S2 units are basically the same and the power output of S2 units will decrease due to the adjustment of energy storage resources in the subsequent periods. In Figure 9-11, it can be seen that compared with S1, the electric output of S2 and S3 are both reduced. The electric output of the unit under the optimized dispatching of S3 has a larger drop. Within its adjustable range, thermal power units and CHP units were reduced by 31.64% and 11.312% respectively.

Heating network characteristics are shown in TABLE 3. In terms of unit heat output, it can be seen from Figure 12 that compared with S1 and S2 which does not consider the delay and attenuation characteristics of the heating network, S3 scheduling consider the network characteristics, and the heat output of the CHP unit is relatively early and lower. In addition, the use of coordinated optimization scheduling considering the network characteristics and energy storage situation makes the heat load peak move forward. It can effectively alleviate the effect caused by the overlap of the heat load and the wind power double peak. Thereby, it can reduce the system operating cost.

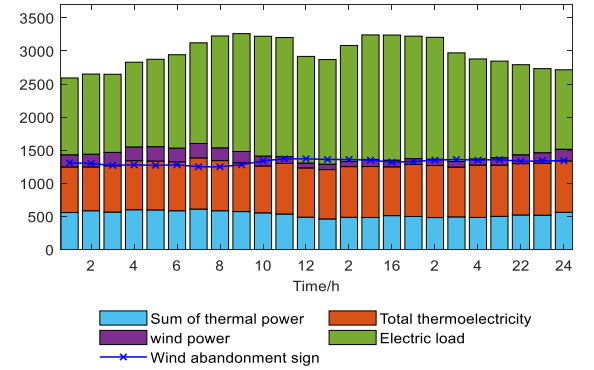

FIGURE 12. The electricity output of each unit in S3 and the sign of wind abandonment.

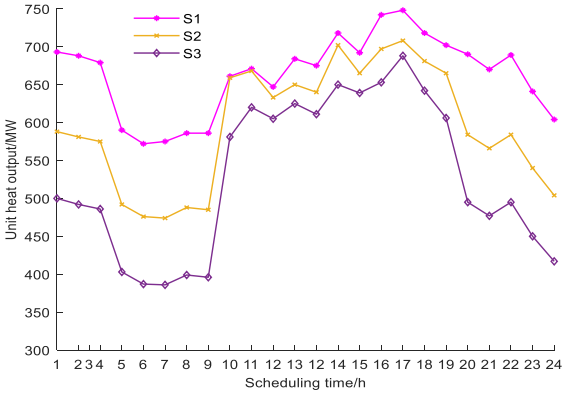

FIGURE 13. Comparison curves of unit heat output under different scenarios.

TABLE 4. Time 9 iteration data analysis.

Symbol	1	2	3	4	5	6
ΔP	0.1	0.06	0.02	0	0	0
ΔH	-38.5	-10	-5	0.03	0	0
λ_p	0.516	0.524	0.533	0.54	0.547	0.547
λ_{h1}	0.43	0.449	0.458	0.465	0.465	0.465
λ_{h2}	0.428	0.425	0.416	0.423	0.423	0.423

3) ANALYSIS OF OPTIMAL SCHEDULING IN S3

Considering the network transmission characteristics and energy storage situation comprehensively, the effectiveness of the double λ iterative algorithm for optimal scheduling of the system can be proved.

The simulation data of ΔP, ΔH, λ_p, λ_{h1} and λ_{h2} at 9 o'clock are shown in Table 4. It can be seen that convergence is reached at the 5th iteration. The system of double Lagrange multiplier converges to the optimal solution at $\lambda_p = 0.547$, $\lambda_{h1} = 0.465$ and $\lambda_{h2} = 0.423$. Network transmission loss P_E, $H_E \approx 0$, and finally reaches the system power balance considering the energy storage situation. The system electric and thermal deviation is minimized, the wind power accommodation is highest, and the operating cost is lowest. TABLE 5 shows the simulation data at each time of the typical day in S3.

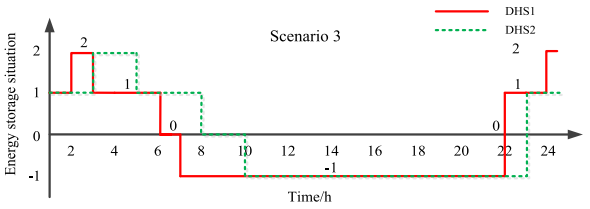

FIGURE 14. Energy storage situation at each moment in S3.

The signs of electricity output and wind power abandonment of each unit in the system during each time period in S3 is shown in Figure 12. According to the simulation's results, the state results of the energy storage system in each period after S3 optimal scheduling are shown in Figure 14. It can be seen that 0 represents the direct thermal state of the electric boiler, 1 represents the heat storage state of the thermal storage tank, and 2 represents the electric storage state, −1 represents release energy state of batteries and heat storage tank. Figure 15 shows the power of the electric boiler, the heat storage of the thermal storage tank, and the power storage of the storage batteries at each time.

During the high wind power generation period of S3, the batteries storage electric and thermal storage tank stores heat. At times 5, 6, and 21, the wind curtailment boundary power satisfies (11), and the energy storage system is the situation of directing thermal from electric boilers. During the day, since the wind curtailment boundary power is less than the system electrical load, all wind power output is used to supply the electrical load. In order to ensure the balance of supply and demand of electric and thermal, storage batteries and heat storage tanks release the energy stored at night to the integrated electric-heat system. On the whole, the use of this optimized scheduling scheme to participate in peak load regulating through the energy storage system can meet the basic electric thermal needs of users.

TABLE 5. Iteration data of typical day in S3.

Time	1	2	3	4	5	6	7	8	9	10	11	12
Convergence or not/times	✓/4	✓/5	✓/4	✓/6	✓/4	✓/5	✓/5	✓/5	✓/5	✓/6	✓/4	✓/4
λ_p	0.524	0.533	0.499	0.54	0.513	0.547	0.527	0.52	0.547	0.498	0.516	0.527
λ_{h1}	0.449	0.458	0.465	0.474	0.469	0.471	0.476	0.475	0.465	0.464	0.478	0.462
λ_{h2}	0.425	0.416	0.423	0.415	0.416	0.43	0.441	0.421	0.423	0.433	0.425	0.426
Time	13	14	15	16	17	18	19	20	21	22	23	24
Convergence or not/times	✓/5	✓/4	✓/4	✓/4	✓/4	✓/5	✓/5	✓/6	✓/5	✓/5	✓/6	✓/5
λ_p	0.531	0.512	0.536	0.515	0.542	0.547	0.547	0.535	0.524	0.53	0.532	0.547
λ_{h1}	0.474	0.474	0.465	0.473	0.473	0.472	0.472	0.472	0.465	0.474	0.464	0.465
λ_{h2}	0.425	0.416	0.423	0.422	0.426	0.416	0.425	0.423	0.36	0.435	0.43	0.424

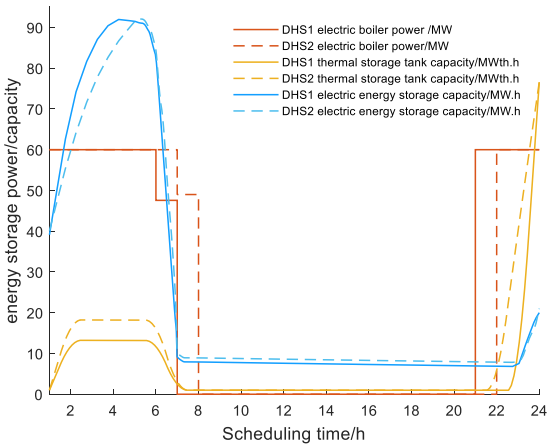

FIGURE 15. Energy storage power/capacity at each time in S3.

Therefore, on the one hand, considering the network transmission characteristics and energy storage situation, the electric and thermal balance of the integrated electric-heat system is realized. On the other hand, the contradiction between the high heat load at night and the large wind power generation is alleviated, and the on-grid power of wind power is increased. The two work together to provide space for wind power and coordinate with the thermal power units to basically realize the full accommodation of wind power and reduce system operating costs.

VIII. CONCLUSION

This paper redefines the integrated electric-heat system with energy storage and proposes a comprehensive dispatching model for coordinated dispatching of electric power and district heating networks. Here use electric boilers, thermal storage tanks and storage batteries, the coordination model considering network transmission characteristics is established as a convex quadratic programming. The double λ iterative algorithm is used to simulate an actual power system and two district heating systems, which indicated the proposed decentralized coordination model and algorithm are efficient and practical. While preserving the dispatch independence between the power system and the heating system, the proposed approach achieves the best solution in a moderate number of iterations. The wind curtailment volume and comprehensive cost of system are significantly reduced. The main conclusions are shown as follows.

1) Electric power network transmission loss, heating network transmission loss and delay will cause deviations in system power. Considering network characteristics can improve system stability and energy supply quality.

2) Wind curtailment boundary power on-off strategy of flexible energy storage resources such as electric boilers, thermal storage tanks and storage batteries can significantly reduce the amount of wind curtailment volume in the system. And it can maximize the use of energy storage capacity, which plays a major role in system optimization and scheduling.

3) The proposed double λ iterative algorithm can effectively solve the coupling optimization problem of wind power accommodation and minimum system cost.

By analyzing multi-objective optimization strategy of integrated electric-heat system based on energy storage situation division and considering the influence of network transmission characteristics on optimal dispatching. Through the effective solution of the double λ iterative algorithm, we can see that this study significantly reduces the wind curtailment volume of the system and brings huge economic benefits. The wind power forecast value and load forecast value in this paper are given, the impact of wind power forecast and load forecast uncertainty on coordinated dispatch has not been studied yet. Future work should study the impact of wind power uncertainty on integrated electric-heat system dispatch.

ABBREVIATIONS

IEHS	Integrated Electric-Heat System
EB	Electric Boiler
HS	Heat Storage Tank
EPS	Electric Power System
DHS	Distribution Heating System
DHN	District Heating Network
CHP	Combined Heat and Power
ECC	Electricity Control Center
HCC	Heating Control Center
R	The total number of wind turbines and thermal units
N	The number of thermal power units
M	The number of heating systems
L	The total number of electric load units
n	The total number of sections of the pipeline
l_g	The length of the heat medium flowing through the pipe$g$ [km]
Δl	The length of the pipe section [m]
d	The inner diameter of the pipe section, [m]
T	The total scheduling period [h]
m	The flow rate of the heat medium [m^3/h]
k	The constant of proportionality
c	The specific heat capacity of the heat medium $[KJ/(kg \cdot^\circ C)]$
ρ	the density of the heat medium [kg/m^3]
$\sum \varepsilon$	The total thermal resistance per kilometer of the pipe between the thermal medium and the surrounding medium [$km \cdot^\circ C/kW$]
λ	The temperature loss coefficient of the unit length of the pipe
$\lambda_{HS,IN}$	The efficiency of the thermal tank device
η_{EB}	The electric heating efficiency of the electric boiler
ζ_{EB}	The power utilization factor of the electric boiler
μ	The thermal loss rate of the heat storage tank

τ	The self-loss rate of the electric power of the storage batteries device
$\gamma_{EES,CHA}$	The charging efficiency of the storage batteries device
$\lambda_{HS,out}$	The release efficiency of the heat storage tank
μ_K	The membership function of the wind power accommodation
μ_P	The membership function of the total system operating cost
δ_1	The acceptable expansion value when the wind power accommodation is the maximum
δ_2	The acceptable expansion value when the total operating cost is the minimum
ξ	The convergence determination coefficient
$\theta_{e,t}$, $\theta_{h,t}$	The voltage phase angles of the bus bar e and bus bar h on the DHS side in period t[rad]
θ_{ij}	The voltage phase angle difference between the i-th and$j$-th node [rad]
ϕ_i^{load}	The magnitude of the heat load at the node i [MWth]
x_{eh}	The direct current resistance of the feeder [Ω]
B_{rm}, B_{ri}, B_{in}	The corresponding elements of the loss coefficient matrix B
T_g	The temperature of the heat medium in the pipe$g$ [°C]
T_0	The ambient temperature around the pipe [°C]
T_i, T_j	The temperature of hot water flowing through nodes i and j respectively [°C]
$T_{g,i}$, $T_{hg,i}$	The water supply temperature and the return water temperature at the node$i$ respectively [°C]
$T_g^{\max}$, $T_g^{\min}$	The upper and lower limits of the water supply temperature in pipe g of the heating network [°C]
$m_g^{\min}$, $m_g^{\max}$	The upper and lower limits [m^3/h]
m_{ij}^h	The water flow of pipe $i-j$ [m^3/h]
m_i^h	The water supply flow of the heat load at the node i [m^3/h]
$q_{g,t}$	The transfer heat [MWth]
$G_{g,t}$	The fluid flow rate inside the pipe section at t[kg/h]
f_K	The wind curtailment power of dispatching system [MW]
f_P	The total operating cost of the system [$]
C_G	The operating cost of the thermal power unit [$]
C_{CHP}	The operating cost of the CHP units of the i-th heating system [$]
C_W	The price of wind power [$/MW]
$A_i \sim F_i$	The cost coefficient of the i-th CHP unit
$a_j \sim c_j$	The cost coefficient of the j-th thermal power unit
k_1, k_2	The weight coefficients
U_i, U_j	The voltage amplitudes of nodes i and j [V]
G_{ij}, B_{ij}	The conductance and susceptance of branchij [S]
$S_{HS,i,t}$	The heat storage capacity of the heat storage tank of the i-th heating system [MWth]
$E_{EES,t}$	The storage capacity of the storage batteries device [MWth]
$E_{EES,\max}$	The maximum capacity of the battery in stable operation The maximum capacity of the battery in stable operation [MWth]
$D_{CHA,t}$, $D_{DIS,t}$, $D_{NW,t}$	The charge, discharge and downtime states of storage batteries
$S_{HS,\min}$, $S_{HS,\max}$	The minimum and maximum capacities of the heat storage tank under stable operation conditions [MWth]
$S_{OH,\min}$, $S_{OH,\max}$	The minimum and maximum values of heat storage and residual heat state [MWth]
$P_{he,t}$	The power flow from h to e on the feeder he in period t [MW]
$P_{CHP,i,t}$	The total electric output of the CHP units of heating system i [MW]
$P_{EB,i,t}$	The output power of the wind turbine to the electric boiler of heating system i [MW]
ΔP	The system electric power deviation [MW]
$P_{G,j,t}$	The electric output of the$j$-th thermal power unit [MW]
$P_{EES,DIS,t}$	The storage batteries output power [MW]
$P_{W,EL,t}$	The power supplied by the wind power plant to the electric load end [MW]
$P_{EES,CHA,t}$	The input power of the storage batteries [MW]
$P_{EL,l,t}$	The demand of the l-th electric load unit [MW]
$P_{E,t}$	The electric transmission loss of the system [MW]
$O_{r,t}$	The electric output of the rth thermal power unit [MW]
$P_{W,t}$	The output of the wind turbine of the integrated electric-heat system [MW]
$P_{W,EES,t}$	The output power of the wind turbine to the storage batteries [MW]

ΔH_i	The sum of the thermal power deviation of the i-th heating system [MWth]
$H_{CHP,i,t}$	The total thermal output of the CHP units of i-th heating system [MWth]
$H_{EB,HL,i,t}$	The thermal power output of the electric boiler direct to heating network of i-th heating system [MWth]
$H_{HS,OUT,i,t}$	The thermal power output released by the heat storage tank to the heating network of the i-th heating system [MWth]
$H_{EV,i,t}$	The heat load of the i-th heating system [MWth]
$H_{E,i,t}$	The heat loss of the i-th heating system [MWth]
ΔH_E	The heat loss of the heat medium flowing through a unit length of pipe [MWth]
$H_{E,t}$	The heat transmission loss of the system [MWth]
$H_{EB,i,t}$	The thermal output by the electric boiler of the i-th heating system [MWth]
$H_{EB,HS,i,t}$	The thermal output by the electric boiler to the heat storage tank of the i-th heating system [MWth]
$H_{HS,IN,i,t}$	The heat storage power of the heat storage tank of the i-th heating system [MWth]
$P_{flag,i,t}$	The wind curtailment boundary power of the i-th heating system [MW]
$P_{CHP,\min i,t}$	The total minimum electric output of CHP unit of the i-th heating system [MW]
$P_{G,\min,t}$	The minimum electric output of thermal power unit [MW]
$P_{PRW,t}$	The predicted output of wind power [MW]
$P_{EB,i,E}$	The rated electric power of the electric boiler of the i-th heating system [MW]
$P_{PW,t}$	The actual output of the wind turbine [MW]
$K_{\max}$	The specific function value when the maximum wind power accommodation is the target [MW]
$P_{\min}$	The specific function value when the minimum total operating cost is the target [MW]
P_i, Q_i	The active and reactive power injections at node i.
$P_i^{\max}$, $Q_i^{\max}$	The allowable active limit transmission power and reactive limit transmission power of branch i, respectively [MW]
$P_{EES,\max,t}^{CHA}$, $P_{EES,\max,t}^{DIS}$	The maximum charge and discharge power of storage batteries [MW]
$P_{EB,\max,t}$	The upper power limit of electric boiler [MW]
$H_{HS,\min}$, $H_{HS,\max}$	The minimum and maximum values of output power of heat storage tanks [MWth]
$P_{G,j,\min}$, $P_{G,j,\max}$	The lower limit and upper limit of the electric power of the j-th thermal power unit [MW]
$P_{PRW,\max,t}$	The predicted output of the wind turbine [MW]
$P_{d,\mathrm{t}}^{line}$	The transmission power of the grid branch d [MW]
$P_d^{line\ \min}$, $P_d^{line\ \max}$	The upper and lower limits of the transmission power of the grid branch d Respectively [MW]

APPENDIX A

A. ESTABLISHMENT OF WIND POWER PREDICTION MODEL BASED ON SIMILAR DAYS AND FEATURE EXTRACTION

1) MATCHING OF SIMILAR DAYS

The main factors affecting the output of wind turbines are wind speed, wind direction, temperature, pressure, relative humidity and other meteorological elements. The sequence of sampling points of these meteorological elements is used to match similar days. The specific steps are shown as follows [35].

(1) Assuming there are N historical days, first the sampling point sequence of each meteorological element of N historical days and forecast days is expressed into $\{i, c_i\}_{i=1.....k}$ form, where i is the serial number arranged in the order of sampling time, and c_i is the instantaneous data, sampling once every 15min, then $k = 96$.

(2) Respectively normalize the sampling point sequence of wind speed, wind direction, temperature, pressure, and relative humidity according to (A1). According to (A2), the discrete Frechet distance d_{ij} of the meteorological element sampling point sequence corresponding to each historical day and the forecast day is calculated, and the obtained distance matrix D is shown as (A3).

$$c_i' = \frac{c_i - \min(c_i)}{\max(c_i) - \min(c_i)} \tag{A1}$$

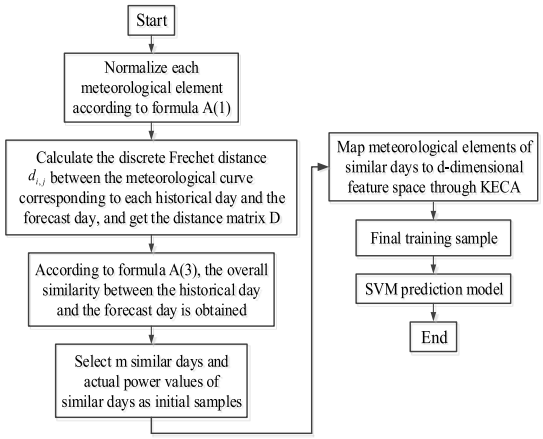

FIGURE 16. Flow chart of wind power forecast.

TABLE 6. Economic characteristic parameters of thermal power unit.

unit	a_i(\$/h)	b_i(\$/MW h)	c_i(\$/M W^{2}h)	Electric power upper limit (MW)	Electric power lower limit (MW)
7	4.9369	0.2762	0.0011	680	320
8	5.9653	0.2608	0.0008	680	275

TABLE 7. Economic Characteristic Coefficient of CHP unit.

unit	A_i(\$/M W^{2}h)	B_i(\$/M Wh)	C_i(\$/MW ^{2}h)	D_i(\$/MW ^{2}h)	E_i(\$/MW h)	F_i(\$/ h)
#1	0.0345	14.5	0.031	0.03	4.2	2650
#2	0.0435	36	0.011	0.027	0.6	1250
#3	0.0345	14.5	0.031	0.03	4.2	2650
#4	0.0435	36	0.011	0.027	0.6	1250
#5	0.0345	14.5	0.031	0.03	4.2	2650
#6	0.0435	36	0.011	0.027	0.6	1250

$$\max \begin{cases} d_E(u_p, u_q) \\ \min \begin{cases} d(< u_1, \ldots, u_{p-1} >, \\ \quad < v_1, \ldots, v_q >) \\ \forall n \neq 1 \\ d(< u_1, \ldots, u_p >, \\ \quad < v_1, \ldots, v_{q-1} >) \\ \forall m \neq 1 \\ d(< u_1, \ldots, u_{p-1} >, \\ \quad < v_1, \ldots, v_{q-1} >) \\ \forall n \neq 1 且 m \neq 1 \end{cases} \end{cases} \tag{A2}$$

$$D = [d_{i,j}] \tag{A3}$$

where $d_E(u_p, v_q)$ is the euclidean distance between two points u_p and v_q. $i = 1, \ldots, 5$ is the ith meteorological element, $j = 1, \ldots, N$ is the jth historical day.

(3) The similarity between each historical day and the forecast day is calculated according to the distance matrix D. In order to characterize the leading role of the key factors affecting wind turbine output in the determination of similar days, the equation is defined by multiplying the overall similarity. The equation is shown as (A4).

$$F_j = \prod_{i=1}^{5} \frac{1}{d_{i,j}} \tag{A4}$$

(4) The$m$ day with the highest similarity among N historical days is selected as the similar day sample of the forecast day.

TABLE 8. CHP unit thermoelectric operable domain parameters.

unit	FOR（CHP）
G_{c1}	（0,63），（121,42），（153,132），（0,187）
G_{c2}	（0,36），（106,22），（122,68），（0,94）
G_{c3}	（0,54），（132,38），（156,98），（0,104）
G_{c4}	（0,45），（101,26），（133,78），（0,112）
G_{c5}	（0,78），（167,32），（187,105），（0,99）
G_{c6}	（0,87），（109,20），（134,56），（0,87）

TABLE 9. Power network transmission line parameters.

line	$P_d^{line\ \min}$	$P_d^{line\ \max}$	line	$P_d^{line\ \min}$	$P_d^{line\ \max}$
1-13	0	130	2-13	0	150
5-13	0	180	6-13	0	210
3-13	0	250	4-13	0	190
7-13	0	180	8-13	0	180
9-13	0	120	14-13	0	220

TABLE 10. Heating network transmission pipeline parameters.

pipeline	l_g	$m_{ij}^{\min}$	$m_{ij}^{\max}$	ΣR	node	$T_{ij}^{\min}$	$T_{ij}^{\max}$
3-13	2.8	0	1500	25	3	90	100
4-13	2.5	0	1200	16	4	90	100
7-13	3.0	0	1300	18	7	90	100
8-13	2.6	0	1400	20	8	90	100
9-13	2.9	0	1800	21	9	90	100
14-13	3.1	0	2000	24	14	90	100

TABLE 11. Related parameters of electric boiler.

Electric boiler manufacturer	Rated evaporation	Rated input power	Thermoelectric ratio
Kawasaki Heavy Industries	28t/h/19.6MWth	60 MW	0.98

TABLE 12. Related parameters of storage batteries and thermal storage tank.

Energy storage type	Rated Capacity	Initial capacity	Self-loss rate	effectiv eness
Thermal storage tank	100 MWh	8 MWh	0.01	0.9
Storage batteries	60 MWh	1MWh	0.001	0.96

2) FEATURE EXTRACTION

There is a complicated non-linear relationship between the power generated by the wind turbine and various influencing factors. The KECA method maps the input data to a

TABLE 13. Electric load and wind power forecast output (MW).

Time period	1	2	3	4	5	6	7	8
Electric load	1108.32	1102.51	1113.27	1106.71	1105.14	1058.89	1450.14	1535.15
Wind power forecast	209.69	217.25	197.52	180.41	171.53	149.43	101.18	79.41
Time period	9	10	11	12	13	14	15	16
Electric load	1655.75	1672.3	1681.18	1430.28	1409.15	1670.2	1816.9	1827.14
Wind power forecast	2.9	0	1800	21	9	90	100	
Time period	17	18	19	20	21	22	23	24
Electric load	1784.81	1759.26	1577.49	1446.72	1376.94	1226.6	1203.52	1136.05
Wind power forecast	60.82	73.64	88.93	106.59	184.41	293.06	308.84	316.77

TABLE 14. The heat load (Mwth) of D HN1 of each period considering the delay and attenuation of the heating network.

Time period	N1	N2	N3	N4	N5	N6	N7	N8	N9	N10	SUM
1	71.33	80.35	74.17	2.36	68.18	67.68	68.24	66.66	68.40	68.40	635.78
2	69.94	78.99	72.77	2.36	67.09	66.77	67.15	65.27	67.36	67.40	625.09
3	68.91	77.69	71.66	2.36	66.95	66.90	67.00	64.29	67.28	67.41	620.45
4	68.87	77.13	71.50	2.36	68.00	68.16	68.02	64.35	68.38	68.58	625.34
5	70.00	77.73	72.54	2.36	69.86	70.07	69.84	65.57	70.25	70.48	638.71
6	71.89	79.35	74.40	2.36	71.88	72.01	71.83	67.49	72.23	72.47	655.91
7	73.88	81.38	76.42	2.36	73.64	73.69	73.58	69.47	73.97	74.19	672.57
8	75.61	83.26	78.19	2.36	75.25	75.29	75.17	71.19	75.57	75.80	687.70
9	77.22	84.90	79.81	2.36	77.05	77.12	76.93	72.81	77.36	77.61	703.18
10	79.03	86.60	81.61	2.36	79.07	79.11	78.93	74.64	79.37	79.63	720.34
11	81.05	88.56	83.64	2.36	80.87	80.74	80.72	76.67	81.12	81.35	737.08
12	82.79	90.53	85.46	2.36	81.80	81.41	81.66	78.37	81.99	82.14	748.50
13	83.63	91.87	86.41	2.36	81.54	80.91	81.42	79.11	81.67	81.74	750.67
14	83.28	92.07	86.17	2.36	80.37	79.66	80.29	78.67	80.49	80.52	743.89
15	82.08	91.19	85.02	2.36	78.97	78.31	78.90	77.43	79.11	79.14	732.50
16	80.69	89.80	83.61	2.36	77.82	77.25	77.76	76.05	77.99	78.04	721.36
17	79.57	88.52	82.45	2.36	76.95	76.42	76.89	74.96	77.13	77.19	712.43
18	78.71	87.56	81.57	2.36	76.04	75.48	76.00	74.10	76.22	76.26	704.32
19	77.80	86.71	80.66	2.36	74.89	74.30	74.87	73.17	75.07	75.09	694.93
20	76.63	85.66	79.51	2.36	73.62	73.06	73.61	71.98	73.81	73.83	684.07
21	75.37	84.39	78.23	2.36	72.51	72.02	72.51	70.72	72.71	72.75	673.57
22	74.28	83.18	77.11	2.36	71.65	71.21	71.65	69.65	71.87	71.92	664.87
23	73.43	82.23	76.24	2.36	70.80	70.33	70.82	68.81	71.02	71.05	657.10
24	72.57	81.42	75.39	2.36	69.66	69.13	69.70	67.93	69.87	69.87	647.89

high-dimensional feature space through a kernel function, extracts nonlinear principal components, and maximizes the information entropy in the original data [36].

Data set $X = [x_1, x_2, \ldots, x_{m\times 96}]$ is selected m similar day data, x_i is expressed as a vector composed of wind speed, wind direction, temperature, pressure, and relative humidity at the same time. The specific steps of feature extraction based on the KECA method are divided into the following 3 steps.

(1) This paper selects the radial basis function as the kernel function of (A5), and constructs the corresponding kernel correlation matrix K. The radial basis function is expressed as (A6).

$$\hat{p}(x) = \frac{1}{N}\sum_{i=1}^{N} k_\sigma(x, x_i) \tag{A5}$$

$$k_\sigma(x_i, x_j) = \exp(-\frac{||x_i - x_j||}{2\sigma^2}) \tag{A6}$$

where $k_\sigma(x, x_i)$ is the kernel function, σ is the width parameter.

(2) This paper carries out eigenvalue decomposition on the kernel matrix K and estimates the quadratic Renyi entropy according to (A7), and arranges the eigenvalues and corresponding eigenvectors of the kernel matrix in descending order of the estimated value.

$$\hat{V}(p) = \frac{1}{N^2}\sum_{i=1}^{N}(\sqrt{\lambda_i} e_i^T I)^2 \tag{A7}$$

(3) The number of non-linear pivots d is determined, mapping the data to the feature subspace formed by the first d eigenvalues and eigenvectors arranged in descending order. According to (A8), we can obtain the generated nonlinear mapping.

$$\Phi_{eca} = U_d \Phi = D_d^{1/2} E_d^T \tag{A8}$$

where D_d is the diagonal matrix formed by the first d eigenvalues selected after sorting the eigenvalues $\lambda_1, \lambda_2, \ldots, \lambda_N$ in descending order, E_d is formed by the corresponding feature vector.

3) PREDICTION MODEL ESTABLISHMENT

Combining the extrapolation effect of similar days, the KECA method can characterize the internal structure of data about

entropy and the advantages of support vector machines in processing small samples and high dimensions. A support vector machine short-term wind power prediction model based on similar days and feature extraction is proposed [37], as is shown in Figure 16.

Taking the wind speed, wind direction, temperature, pressure, relative humidity, and power at the corresponding time of m similar days as the initial sample set, the initial samples of these 5 meteorological elements through the KECA method is analyzed, and the nonlinear principal elements as the SVM model is extracted. The input and output is the actual power value at the corresponding time to complete the training of the SVM prediction model. When making a prediction, it is necessary to map the weather data of the forecast day, namely wind speed, temperature, humidity, pressure, and relative humidity, to the feature subspace generated by KECA according to (A9), and use it as the input for the prediction.

$$Y_{new} = D_d^{-1/2} E_d^T K(x, x_{new}) \tag{A9}$$

APPENDIX B

See Tables 6–14.

REFERENCES

[1] J. Li, J. Fang, Q. Zeng, and Z. Chen, "Optimal operation of the integrated electrical and heating systems to accommodate the intermittent renewable sources," *Appl. Energy*, vol. 167, pp. 244–254, Apr. 2016, doi: 10.1016/j.apEnergy.2015.10.054.

[2] J. F. Rist, M. F. Dias, M. Palman, D. Zelazo, and B. Cukurel, "Economic dispatch of a single micro-gas turbine under CHP operation," *Appl. Energy*, vol. 200, pp. 1–18, Aug. 2017, doi: 10.1016/j.apEnergy.2017.05.064.

[3] H. C. Wang, D. M. Lin, R. Lahdelma, and X. L. Li, "Developing a multicriteria decision support framework for CHP based combined district heating systems," *Appl. Energy*, vol. 205, pp. 345–368, Jul. 2017, doi: 10.1016/j.apEnergy.2017.07.016.

[4] L. Ye, C. Zhang, Y. Tang, W. Zhong, Y. Zhao, P. Lu, B. Zhai, H. Lan, and Z. Li, "Hierarchical model predictive control strategy based on dynamic active power dispatch for wind power cluster integration," *IEEE Trans. Power Syst.*, vol. 34, no. 6, pp. 4617–4629, Nov. 2019, doi: 10.1109/TPWRS.2019.2914277.

[5] X. Dui, G. Zhu, and L. Yao, "Two-stage optimization of battery energy storage capacity to decrease wind power curtailment in grid-connected wind farms," *IEEE Trans. Power Syst.*, vol. 33, no. 3, pp. 3296–3305, May 2018, doi: 10.1109/TPWRS.2017.2779134.

[6] N. Zhang, X. Lu, M. B. McElroy, C. P. Nielsen, X. Y. Chen, and Y. Deng, "Reducing curtailment of wind electricity in China by employing electric boilers for heat and pumped hydro for energy storage," *Appl. Energy*, vol. 184, pp. 987–994, Jun. 2016, doi: 10.1016/j.apEnergy.2015.10.147.

[7] M. G. Nielsen, J. M. Morales, M. Zugno, T. E. Pedersen, and H. Madsen, "Economic valuation of heat pumps and electric boilers in the danish energy system," *Appl. Energy*, vol. 167, pp. 189–200, Apr. 2016, doi: 10.1016/j.apEnergy.2015.08.115.

[8] Z. H. Wang, L. Yang, C. G. Tian, and G. Q. Li, "The energy optimization of the combined system of wind power—Electric energy storage—Heat storage electric boiler considering wind power consumption," *Chin. J. Electr. Eng.*, vol. 37, pp. 137–143, Sep. 2017, doi: 10.13334/0258-8013.J.pcsee.170475.

[9] Z. Li, W. Wu, M. Shahidehpour, J. Wang, and B. Zhang, "Combined heat and power dispatch considering pipeline energy storage of district heating network," *IEEE Trans. Sustain. Energy*, vol. 7, no. 1, pp. 12–22, Jan. 2016, doi: 10.1109/TSTE.2015.2467383.

[10] Z. K. Yi and Z. M. Li, "Combined heat and power dispatch that takes into account the thermal inertia of heat storage and heating area of the heating network," *Power Syst. Technol.*, vol. 42, no. 5, pp. 1378–1384, Feb. 2018, doi: 10.13335/j.1000-3673.pst.2017.2703.

[11] G. B. Zhang, J. H. Zhang, R. J. Guo, Z. P. Gao, and Y. G. Niu, "Scheduling strategy for combined cooling-heating-power generation system based on adaptive chaotic particle swarm optimization algorithm," *Modern Electr. Power*, vol. 37, no. 06, pp. 551–558, Dec. 2020, doi: 10.19725/j.cnki.1007-2322.2019.1070.

[12] S. Wang and M. Z. Li, "Research on power system load forecasting based on improved particle swarm optimization," *Electron. Manuf.*, vol. 19, pp. 89–92, Sep. 2020, doi: 10.16589/j.cnki.cn11-3571/tn.2020.19.030.

[13] B. Mohammadi-Ivatloo, M. Moradi-Dalvand, and A. Rabiee, "Combined heat and power economic dispatch problem solution using particle swarm optimization with time varying acceleration coefficients," *Electr. Power Syst. Res.*, vol. 95, pp. 9–18, Feb. 2013, doi: 10.1016/j.epsr.2012.08.005.

[14] M. Y. Gong, "Research on optimal control of centralized electric heating system based on genetic algorith," M.S. thesis, Dept. Electron. Eng., Harbin Inst. Technol., Harbin, China, 2020.

[15] Y. H. Song, C. S. Chou, and T. J. Stonham, "Combined heat and power economic dispatch by improved ant colony search algorithm," *Electr. Power Syst. Res.*, vol. 52, no. 2, pp. 21–115, Jun. 1999, doi: 10.1016/S0378-7796(99)00011-5.

[16] E. Khorram and M. Jaberipour, "Harmony search algorithm for solving combined heat and power economic dispatch problems," *Energy Convers. Manage*, vol. 52, no. 2, pp. 1550–1554, Jun. 2010, doi: 10.1016/j.enconman.2010.10.017.

[17] X. S. Jiang, Z. X. Jing, Y. Z. Li, Q. H. Wu, and W. H. Tang, "Modelling and operation optimization of an integrated energy based direct district water-heating system," *Energy*, vol. 64, pp. 375–388, Jun. 2014, doi: 10.1016/j.Energy.2013.10.067.

[18] J. H. Zheng, J. J. Chen, Q. H. Wu, and Z. X. Jing, "Multi-objective optimization and decision making for power dispatch of a large-scale integrated energy system with distributed DHCs embedded," *Appl Energy*, vol. 154, pp. 369–379, Jun. 2015, doi: 10.1016/j.apenergy.2015.05.023.

[19] H. M. Yang, T. L. Xiong, J. Qiu, D. Qiu, and Z. Y. Dong, "Optimal operation of DES/CCHP based regional multi-energy prosumer with demand response," *Appl Energy*, vol. 167, pp. 353–365, Jun. 2016, doi: 10.1016/j.apenergy.2015.11.022.

[20] Z. Pan, Q. Guo, and H. Sun, "Feasible region method based integrated heat and electricity dispatch considering building thermal inertia," *Appl. Energy*, vol. 192, pp. 395–407, Apr. 2017, doi: 10.1016/j.apenergy.2016.09.016.

[21] M. Cococcioni, A. Cudazzo, M. Pappalardo, and Y. D. Sergeyev, "Solving the lexicographic multi-objective mixed-integer linear programming problem using branch-and-bound and grossone methodology," *Commun. Nonlinear Sci. Numer. Simul.*, vol. 84, May 2020, Art. no. 105177, doi: 10.1016/j.cnsns.2020.105177.

[22] C. M. Zheng, B. N. Huang, Z. X. Wang, and Q. Y. Sun, "Multi-objective optimal dispatch of electric and heating integrated energy system considering network transmission loss," *Power Syst. Technol.*, vol. 44, no. 1, pp. 141–154, Jan. 2020, doi: 10.13335/j.1000-3673.pst.2019.1334.

[23] Y. A. Shaabani, A. R. Seifi, and M. J. Kouhanjani, "Stochastic multi-objective optimization of combined heat and power economic/emission dispatch," *Energy*, vol. 141, pp. 1892–1904, Dec. 2017, doi: 10.1016/j.Energy.2017.11.124.

[24] A. M. Salman, Y. Li, and M. G. Stewart, "Evaluating system reliability and targeted hardening strategies of power distribution systems subjected to hurricanes," *Rel. Eng. Syst. Saf.*, vol. 144, no. 3, pp. 319–333, Dec. 2015, doi: 10.1016/j.res.2015.07.028.

[25] J. M. Boggess, G. W. Becker, and M. K. Mitchell, "Storm & flood hardening of electrical substations," in *Proc. IEEE PES T&D Conf. Expo.*, Chicago, IL, USA, Apr. 2014, pp. 1–5,

[26] Y. Z. Wang and X. Liu, "Hot water heating system," in *Heating Engineering*, vol. 3, 3nd ed. Beijing, China: Mechanical Industry Press, 2007, pp. 266–270.

[27] W. Gu, S. Lu, and J. Wang, "Modeling of the heating network for multi-district integrated energy system and its operation optimization," *Proc. CSEE*, vol. 37, no. 5, pp. 1305–1315, Jan. 2017, doi: 10.13334/j.0258-8013.pcsee.160991.

[28] X. Li, W. Li, R. Zhang, T. Jiang, H. Chen, and G. Li, "Collaborative scheduling and flexibility assessment of integrated electricity and district heating systems utilizing thermal inertia of district heating network and aggregated buildings," *Appl. Energy*, vol. 258, Jan. 2020, Art. no. 114021, doi: 10.1016/j.apEnergy.2019.114021.

[29] P. Singh and J. S. Lather, "Power management and control of a grid-independent DC microgrid with hybrid energy storage system," *Sustain. Energy Technol. Assessments*, vol. 43, Feb. 2021, Art. no. 100924, doi: 10.1016/j.seta.2020.100924.
[30] H. A. Aalami and S. Nojavan, "Energy storage system and demand response program effects on stochastic energy procurement of large consumers considering renewable generation," *IET Gener., Transmiss. Distrib.*, vol. 14, no. 24, p. 6040, Dec. 2020, doi: 10.1049/iet-gtd.2020.1476.
[31] J. L. Deng, L. X. Hu, and J. J. Li, "The mechanism and economic analysis of wind absorption and abandonment using two-stage heating network electric boiler peak shaving," *Autom. Electr. Power Syst.*, vol. 40, no. 18, pp. 41–47, Sep. 2016, doi: 10.7500/AEPS20151001001.
[32] T. Guo, M. I. Henwood, and M. van Ooijen, "An algorithm for combined heat and power economic dispatch," *IEEE Trans. Power Syst.*, vol. 11, no. 4, pp. 1778–1784, Nov. 1996, doi: 10.1109/59.544642.
[33] T. Xu, W. Wu, W. Zheng, H. Sun, and L. Wang, "Fully distributed quasi-Newton multi-area dynamic economic dispatch method for active distribution networks," *IEEE Trans. Power Syst.*, vol. 33, no. 4, pp. 4253–4263, Jul. 2018, doi: 10.1109/TPWRS.2017.2771950.
[34] J. Huang, Z. Li, and Q. H. Wu, "Coordinated dispatch of electric power and district heating networks: A decentralized solution using optimality condition decomposition," *Appl. Energy*, vol. 206, pp. 1508–1522, Nov. 2017, doi: 10.1016/j.apEnergy.2017.09.112.
[35] D. Ganger, J. Zhang, and V. Vittal, "Statistical characterization of wind power ramps via extreme value analysis," *IEEE Trans. Power Syst.*, vol. 29, no. 6, pp. 3118–3119, Nov. 2014, doi: 10.1109/TPWRS.2014.2315491.
[36] M. Yesilbudak, "Clustering analysis of multidimensional wind speed data using k-means approach," in *Proc. IEEE Int. Conf. Renew. Energy Res. Appl. (ICRERA)*, Nov. 2016, pp. 961–965, doi: 10.1109/ICRERA.2016.7884477.
[37] J. Yan, C. Z. Xu, Y. Q. Liu, S. Han, and L. Li, "Short-term wind power prediction method based on similar days of wind speed cloud model," *Autom. Electr. Power Syst.*, vol. 42, no. 6, pp. 53–59, Dec. 2017, doi: 10.7500/AEPS20170605001.

XINRUI LIU (Member, IEEE) received the B.S., M.S., and Ph.D. degrees in control theory and control engineering from Northeastern University, Shenyang, China, in 2003, 2006, and 2010, respectively. She is currently an Associate Professor with the College of Information Science and Engineering, Northeastern University. Her current research interests include research and application of fuzzy control of interconnected large systems, cyber-physical systems, self-healing control of intelligent power transmission and distribution systems, and multi-energy complement control.

FUJIA ZHANG received the B.Sc. degree in electrical engineering from Pingdingshan University (PDSU), Pingdingshan, China, in 2018. She is currently pursuing the M.Eng. degree with Northeastern University (NEU), China. Her research interests include electric thermal integrated energy and interconnection of distributed resources.

QIUYE SUN (Senior Member, IEEE) received the B.S. degree in power system and its automation from Northeast Dianli University, Jilin City, China, in 2000, and the M.S. degree in power electronics and drives and the Ph.D. degree in control theory and control engineering from Northeastern University, Shenyang, China, in 2004 and 2007, respectively. Since 2014, he has been a Full Professor with the College of Information Science and Engineering, Northeastern University. He has authored and coauthored over 280 journal and conference papers, six monographs, and co-invented 90 patents. His research interests include optimization analysis technology of power distribution networks, network control of distributed generation systems, microgrids, and energy internet.

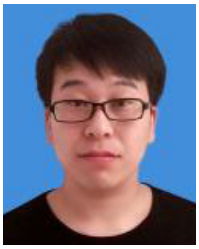

WEIYANG ZHONG received the B.E. degree in inorganic non-metallic materials engineering from Liaoning University (LNU), China, in 2017. He is currently pursuing the M.Eng. degree with Northeastern University (NEU), China. His research interests include electric thermal integrated energy and interconnection of distributed resources.